Sustaining Earth's magnetic dynamo

Maylis Landeau, Alexandre Fournier, Henri-Claude Nataf, David Cébron, Nathanaël Schaeffer

This document is the accepted manuscript corresponding to the article
https://doi.org/10.1038/s43017-022-00264-1
Sustaining Earth's magnetic dynamo. Nat Rev Earth Environ 3, 255–269 (2022).

Sustaining Earth's magnetic dynamo

Maylis Landeau[1], Alexandre Fournier[1], Henri-Claude Nataf[2], David Cébron[2], and Nathanaël Schaeffer[2,†]

[1]Université de Paris, Institut de Physique du Globe de Paris, CNRS, Paris, France
[2]Université Grenoble Alpes, CNRS, ISTerre, Grenoble, France
[†]e-mail: nathanael.schaeffer@univ-grenoble-alpes.fr

ABSTRACT

Earth's magnetic field is generated by fluid motions in the outer core. This geodynamo has operated for over 3.4 Gyrs. However, the mechanism that has sustained the geodynamo for over 75% of Earth's history remains debated. In this Review, we assess the mechanisms proposed to drive the geodynamo (convection, precession and tides) and their ability to match geomagnetic and paleomagnetic observations. Flows driven by precession are too weak to drive the geodynamo. Flows driven by tides could have been strong enough in the early Earth, prior to 1.5 Ga, when tidal deformation and Earth's spin rate were larger than today. Evidence that the thermal conductivity of Earth's core could be as high as 250 $\mathrm{W\,m^{-1}\,K^{-1}}$ questions the ability of convection to maintain the dynamo for >3.4 Gyrs. Yet, convection can supply enough power to sustain a long-lived geodynamo if the thermal conductivity is lower than 100 $\mathrm{W\,m^{-1}\,K^{-1}}$. Exsolution of light elements from the core increases this upper conductivity by 15% to 200%, based on the exsolution rates reported so far. Convection, possibly aided by the exsolution of light elements, remains the mechanism most likely to have sustained the geodynamo. The light-element exsolution rate, which remains poorly constrained, should be further investigated.

Key points:

- Numerical models of the geodynamo driven by thermo-chemical convection account for most of the observed properties of the present geodynamo.
- The thermal conductivity in Earth's core remains debated, with published values ranging between 20 and 250 $\mathrm{W\,m^{-1}K^{-1}}$. With a conductivity as high as 250 $\mathrm{W\,m^{-1}K^{-1}}$, motionless heat transport prevails in the core, hence convection cannot sustain Earth's magnetic dynamo for 3.4 Gyrs.
- Still, thermo-chemical convection due to the slow cooling of Earth supplies enough power to the geodynamo when the thermal conductivity is lower than 100 $\mathrm{W\,m^{-1}K^{-1}}$. The exsolution of light elements increases this limit only marginally or by up to a factor 3 depending on the exsolution rate.
- Flows driven by precession are too weak to drive the geodynamo.
- Flows driven by tides could have been strong enough prior to 1.5 Ga, when tidal deformation and Earth's spin rate were larger than today. This calls for further investigation of tidally-driven dynamos.

Website summary: The mechanisms that sustain Earth's long-lived geodynamo remain under scrutiny. This Review assesses the potential candidates – convection, precession and tides – revealing that convection, possibly helped by the exsolution of light elements, is the most likely scenario.

1 Introduction

The Earth's surface is immersed in a magnetic field that is mainly a dipole. The geomagnetic field deviates charged particles from the Sun, which may help to protect Earth's atmosphere from erosion by solar winds[1–3]. Humans have used magnetic compasses to navigate the oceans and continents for thousands of years. Other animals, including sea turtles and salmons, are also suspected to use the magnetic field for navigation[4,5]. Magnetotactic bacteria, which swim along magnetic field lines[6,7], rely on Earth's magnetic field to migrate up and down in the sediment column.

The magnetic field is hence an essential aspect of Earth. Yet, the origin of this field long remained a mystery. In 1919, it was hypothesised that the geomagnetic field originates from flow motions of conducting material inside the Earth through the

so-called *dynamo effect*[8] (box 1). Over a century later, it is now widely accepted that the geodynamo operates in the outer core, which is made of flowing liquid metal (figure 1a)[9].

The most accepted scenario to drive turbulent core flows and the geodynamo is natural convection[9] due to the slow cooling of the Earth (figure 1b). Numerical simulations of a convection-driven geodynamo produce a magnetic field that resembles that of the Earth[10] and they are coming close to the conditions of Earth's core[11–15]. Therefore, the behaviour of the geomagnetic field at Earth's surface can be explained by the convective dynamics deep inside the core[14,15].

Magnetized rocks indicate that the geodynamo is at least 3.4 Gyrs old[16]. Whether convection can sustain the geodynamo for such a long time critically depends on the thermal conductivity of the core[17]. However, the value of core conductivity is highly debated, with published values[18–26] ranging between 20 and 250 $\mathrm{W\,m^{-1}K^{-1}}$. With high conductivity values of $100-250\ \mathrm{W\,m^{-1}K^{-1}}$ found by experimental and numerical investigations[23–26], much of the core heat flow would escape by conduction, leaving little to drive thermal convection, especially in the distant past when the core was fully molten[17,27,28]. This disconcerting result, coined the *new core paradox*[17], motivated the search for other mechanisms to drive the geodynamo.

A possible mechanism is the exsolution of light elements from the core (figure 1c). Exsolution leaves behind a denser liquid, which produces natural convection and helps to sustain a convective geodynamo[29–31]. Tides and precession are also alternative mechanisms[32–35] that can produce turbulent flows in the outer core[36–39], and hence could drive a dynamo (figure 1de). Advances in simulations of precession-driven dynamos since the 2000s[40–43] have generated interest in a geodynamo powered by orbital forcing[44]. However, it remains debated whether the exsolution of light elements, precession or tides produce flows that are strong enough to solve the new core paradox.

In this review, we compare the candidate driving mechanisms for the geodynamo - convection, precession and tides (figure 1bcde). We first summarise the main properties of Earth's dynamo that are deduced from geomagnetic and paleomagnetic observations. For each driving mechanism, we discuss the latest simulations and evaluate their compliance with the present-day geomagnetic field. We then examine whether the power or kinetic energy produced by each mechanism over geological time can sustain the long-lasting magnetic field observed in paleomagnetic data. In the future, better understanding of the early geodynamo requires further investigation of the flow and magnetic fields produced by convection or tides in a fully liquid core, with no inner-core. Additional constraints on the rate at which light elements have exsolved from the core throughout Earth's history are also needed.

2 Geomagnetic and paleomagnetic observations

Our understanding of Earth's dynamo rests on the analysis of the present and past geomagnetic field. The direct observation of the geomagnetic field since the seventeenth century places important constraints on the working of the geodynamo on interannual to secular time scales. Paleomagnetic studies provide additional information on the mechanisms driving the geodynamo on millennial to geological time scales.

2.1 From the Age of Sail to the present day

Nowadays, satellites and ground-based observatories provide us with a global and time-dependent map of the Earth's magnetic field[45]. The main field, of about 50 μT at the Earth's surface[46], is generated in the Earth's core[47]. This field is dominated by a dipole slightly tilted with respect to the axis of rotation of the Earth, with a dipole moment of about 8×10^{22} A m^2.

To trace the variations of the geomagnetic field, one has to recourse to the archives of magnetic observatories, some of which date back to the seventeenth century. Additional information can be obtained from mariners' logbooks, in which the direction of the magnetic north pole was reported during voyages[48]. This information is available from the end of the sixteenth century onward. The rate of change of the geomagnetic field, called the *geomagnetic secular variation*[49], displays 6 yrs period oscillations during the last century[50]. These oscillations reflect the propagation of hydromagnetic waves, called *Alfvén waves*, in the outer core. As their propagation speed is proportional to the magnetic field, the field strength deep in the core can be estimated to ~ 4 mT[51]. This value is about 10 times the field strength at the core-mantle boundary (CMB), and it corresponds to a magnetic energy[52] of $\sim 10^{21}$ J inside the core.

Beyond waves, flows inside the core transport magnetic field lines. This process explains most of the decadal to secular fluctuations of the geomagnetic signal[53]. These variations suggest a large-scale velocity of $\sim 3\times10^{-4}$ m s^{-1} below the core surface. Assuming that this figure is representative of the flow in the bulk of the outer core yields a kinetic energy of 8×10^{16} J, about 10^4 times smaller than the magnetic energy[51].

2.2 Over geological time

Prior to the sixteenth century, observations of the geodynamo rely on the remnant magnetization carried by rocks or archeological recorders[54,55]. In the laboratory, it is possible to recover the direction or amplitude of the geomagnetic field that reigned when the magnetization was acquired. These indirect measurements allow geologists to determine the motion of continents over hundreds of millions of years[56]. They also open a window on the behaviour of the geodynamo over several billions of years.

One of the most fundamental question for paleomagnetic studies is the age of the geodynamo. Magnetic inclusions in extremely old minerals from South Africa provide robust evidence that the geodynamo was active 3.4 Gyrs ago[16]. Analyses of samples from Greenland suggest that the geodynamo had started 3.7 Gyrs ago[57]. An even older dynamo record from 4.2 Gyrs ago has been proposed[58] but this finding remains controversial[59].

The geodynamo has evolved on multiple time scales (figure 2). Over the last millennia, the dipole strength varied between 0.7 and 1.4 times its present-day value (figure 2a). Earth's magnetic field has frequently reversed its polarity (figure 2b,c). The frequency of reversals is highly variable on time scales of a hundred million years[54,60]. During the last few million years, the field reversed 4 times per million year, but further in the past, there were periods of several million years with no reversal (figure 2c). Thanks to the increase in quality and number of paleointensity measurements, it is now possible to search for long-term trends in the paleointensity signal over the last 3 billion years[61–63] (figure 2d). Paleomagnetic data show that the geodynamo produced a strong, seemingly dipole-dominated field, with a moment of $5 \pm 2 \times 10^{22}$ A m^2 during more than 75% of Earth's history[61,62,64,65].

3 Driving mechanisms

In this section, the possible driving mechanisms for the geodynamo are introduced. Their ability to produce a field resembling the present-day geomagnetic field are assessed in the light of numerical simulations.

3.1 Cooling and inner-core growth

The Earth is cooling down. At present, a heat flow of 46 ± 3 TW escapes at the solid Earth's surface[66], while ~ 18 TW are produced by the disintegration of radioelements within the mantle and crust[67,68] and less than 2 TW by radioelements within the core[27].

The cooling of the Earth is the most accepted mechanism to drive the present-day geodynamo[52,69–71]. As the core slowly cools down, the solid inner core grows, releasing latent heat and light elements[72] at the inner-core boundary (figure 1b). The light fluid rises to the CMB, thereby generating vigorous plumes in the outer core[73] (figure 1a). Meanwhile, as heat leaves the core, colder fluid forms at the CMB and sinks downwards (figure 1b).

Earth's rotation strongly influences these convective motions, which take the form of swirling columns aligned with the rotation axis[74–78] (figure 1a). These swirling flows are prone to dynamo action[9] (box 1). The dipolar geomagnetic field, and its close alignment with the rotation axis, are well explained by these columnar motions[79] (figure 1a).

The first self-consistent numerical dynamo driven by convection was obtained in 1995[80,81]. Simulations soon could account for several features of the observed geomagnetic field[10,82] (figure 3a), including its dipolar dominance, patches of enhanced magnetic field at high latitudes (figures 3b and 3c) and polarity reversals (table in box 2). With the increase in computing power, a large number of simulations could be run. Parametric exploration led to the derivation of scaling laws that relate the power from convection to the magnetic and flow intensity[83,84]. These laws predict a magnetic field intensity of ~ 1 mT inside the core, in line with the estimates from geomagnetic observations (section 2.1).

In turbulent geodynamo simulations[11,12,15], the intensity of the magnetic field inside the core is about 10 times stronger than at the CMB, as inferred for the Earth[51]. The hierarchy of dominant forces is now the same as in Earth's core[12,15,85]. Simulations also produce fast waves interacting with the slower convective motions[14,15,86]. Thanks to results from these simulations, abrupt changes in the surface field (termed geomagnetic jerks) are now interpreted as the arrival of waves that are excited by convective plumes in the core[14,15]. Convective dynamos generate a time evolving field that explains most of the observed secular variations (table in box 2).

3.2 The exsolution of light elements

In addition to iron and nickel, the outer core contains lighter elements, including Si, O, S, H or Mg[72]. The partitioning of some light elements in iron increases with temperature[30,87–89]. The Earth's core experienced high temperatures > 5000 K during its formation, when large impacts brought new metal and silicates to the growing planet[90,91]. After each collision, the newly brought metal sank into the mantle, where it incorporated light elements, and then merged with the Earth's core[30,72].

Subsequently, on geological time, the core cooled down. For each light element with a given initial concentration, there is a critical temperature below which exsolution starts[29–31], leaving an iron-rich liquid that sinks into the deeper core. These convective motions can contribute to the geodynamo not only today but also in the distant past, prior to the growth of the inner core[29–31] (figure 1c).

Which light element exsolves from the core is still debated. Some high-pressure experiments and molecular dynamics simulations suggest that magnesium oxides MgO would be the first exsolved species[30,31,92,93] while others favour silicon oxides SiO_2[89,94]. One study[95] found that the liquid Fe-Si-O system separates into immiscible liquid alloys as the core cools down, instead of exsolving SiO_2 oxides, but the robustness of these results has been questioned[92].

Of paramount importance is the depth at which exsolution starts. Were it at the bottom, a dense iron-rich liquid would accumulate there, generating a stable stratification but no convection. Several studies[88,93] find that the exsolution of MgO starts at the top of the core, and hence can drive convection. For SiO_2, the uncertainties on the solubility curve are still too large to determine the depth at which its exsolution starts[89].

The exsolution of light elements at the top of the core can drive the geodynamo through convection. Thus, the results from dynamo simulations driven by thermo-chemical convection (section 3.1) to some extent apply to exsolution. In a dynamo simulation, exsolution can be modelled by volumetric buoyancy sources that are balanced by a buoyancy flux at the CMB. However, only few[96–98] have investigated this configuration, which is also appropriate for thermal convection driven by the slow cooling of the core prior to the growth of an inner core.

3.3 Precession and tides

Precession and tides can also trigger flow motions and dynamo action. Precession, a slow variation of the orientation of Earth's rotation axis (figure 1d), forces the fluid core to rotate along a different axis than the mantle[99–101]. At present, precession induces a diurnal differential motion of about 60 m at the CMB and a velocity $u_p \sim 4$ mm s^{-1}. Because the core is not perfectly spherical, precession also triggers a weak secondary flow[102] of amplitude $u_p f_\mathrm{p}$, where $f_\mathrm{p} \approx 1/400$ is the CMB ellipticity[103]. Tides produce a diurnal CMB deformation of ellipticity $f_\mathrm{t} \approx 10^{-7}$ moving around the core at speed $u_t = 250$ m s^{-1} (figure 1e). These flows do not produce magnetic fields by themselves (box 1)[41,104]. Still, instabilities near the boundary or in the bulk core can lead to turbulent flows and dynamo action[40,43,105].

Simulations of dynamos driven by precession[40,43,105] or tides[106] have yet to provide scaling laws for the intensity of the magnetic field. Furthermore, the magnetic field is always weak and small-scale[43,105,106] (figure 3d), and hence very different from the dipolar geomagnetic field (figure 3a). In ellipsoids, simulations of large-scale magnetic fields were initially reported[107], but their validity was subsequently questioned[108]. Currently, it is not known whether orbital forcings are able to produce a large-scale, dipolar magnetic field with an amplitude compatible with that of the geomagnetic field. Lowering viscosity in future simulations might answer this question.

While low viscosity is hard to reach in simulations, it is a feature of laboratory experiments that use liquid sodium (see Supplementary Fig.1)[109–112]. No experimental dynamos driven by precession or tides have yet been published. However, all eyes are on the DRESDYN dynamo experiment, which is currently being built and will be driven by precession[113].

4 Sustaining a convective geodynamo

Paleomagnetic observations indicate an active geodynamo during the last 3.4 Gyrs. In this section, the energetics of the core are used to assess whether convection can power such a long-lived dynamo.

4.1 Thermal conductivity

Mantle convection sets the heat flow that escapes from the core[52,66]. A substantial portion of this heat is transported by thermal conduction in the core and does not participate to core convection. The higher the conducted heat flow, the lower the power available for the geodynamo.

The conducted heat flow, often called *isentropic* heat flow, reads at the CMB

$$Q_\mathrm{is} = -k \, \frac{\partial T}{\partial r} \, \mathscr{A}, \tag{1}$$

where the temperature gradient is

$$\frac{\partial T}{\partial r} = -\frac{\alpha \, g \, T}{C_P} \tag{2}$$

in an isentropic, well-mixed core[114], k is the thermal conductivity, $\mathscr{A}$ the area of the CMB, α the coefficient of thermal expansion, C_P the specific heat capacity, and g the acceleration of gravity at the CMB.

The isentropic heat flow is therefore proportional to the thermal conductivity k, whose range of published values broadened since the early 2010s'[23–25,115]. Direct experimental measurements suggest low values[18–20] of k between 20 and 46 W m^{-1} K^{-1}, in line with older estimates[21,22], while other studies find larger values of k[23–26,116] between 90 and 250 W m^{-1} K^{-1}. This scatter is partly due to the relation between electrical and thermal conductivity which remains to be clarified at high pressure and temperature[117]. Adding light elements in the core lowers the thermal conductivity[20], further increasing its uncertainty.

Here, the impact of two end-member values on the geodynamo are examined: a high-conductivity $k \simeq 100$ W m^{-1} K^{-1}, which results in a conducted heat flow $Q_\mathrm{is} \simeq 15$ TW, and a low-conductivity $k \simeq 40$ W m^{-1} K^{-1}, which results in $Q_\mathrm{is} \simeq 6$ TW.

4.2 Convection can power the current geodynamo

In the Earth's core, the magnetic field generates electric currents, which dissipate energy by ohmic heating. Theory, numerical models and experiments suggest that the power lost today by ohmic dissipation is on the order of 1 TW[9,118,119]. The driving mechanism of the geodynamo must therefore supply enough power to balance this ohmic dissipation.

From the energy and entropy budgets of the core, one can estimate the power originating from convection[27,28,120–123]. As shown in this section, a high-conductivity value does not prevent a convective dynamo at the present day. Regardless of the exact value of the thermal conductivity, the outer core still solidifies into an inner core, driving convection and dynamo action.

At the CMB, thermal convection is possible when the core heat flow $Q_{\rm cmb}$ exceeds the conducted heat flow $Q_{\rm is}$. The mass anomaly flux that drives convection at this boundary is[120,121]

$$F_o = \frac{\alpha}{C_p}(Q_{\rm cmb} - Q_{\rm is}). \tag{3}$$

At the base of the outer core, the slow solidification of the inner core drives convection with a mass anomaly flux[120,121]

$$F_i = 4\pi {r_i}^2 \dot{r}_i \left(\Delta\rho + \frac{\alpha\,\rho\,L}{C_p} \right), \tag{4}$$

where ρ is the mean density of the outer core, $\Delta\rho$ the density deficit due to the release of light elements, r_i the inner-core radius and L is the latent heat released by the freezing of the inner core. Equation (4) assumes an isentropic heat flow through the inner-core boundary[120]. The two terms in equation (4) describe the flux of light elements due to inner-core growth and the flux of latent heat. Both are proportional to the inner-core growth rate $\dot{r}_i$. The growth rate can be estimated from the energy balance of the core. After the onset of inner-core growth, this balance reads[124]

$$Q_{\rm cmb} = \dot{r}_i P(r_i) + Q_r, \tag{5}$$

where the function P gathers the contributions from latent heat release at the inner-core boundary, gravitational energy release, and cooling of the core, which are all functions of r_i[124], and Q_r is the radiogenic heat production term. The heat flow through the CMB, $Q_{\rm cmb}$, must be balanced by those contributions internal to the core. At the present day, assuming $Q_r = 0$, the growth rate is $\dot{r}_i \simeq 600 \pm 250$ km Gyr^{-1} [27] and F_i is in the range $1\times10^5 - 3\times10^5$ kg s^{-1}. Differences in the function P between studies propagate as an uncertainty of 30% on the age of the inner core.

The convective power $\Phi_{\rm conv}$ available for the dynamo is approximated by[120,121]

$$\Phi_{\rm conv} = F_i(\bar{\psi} - \psi_i) + F_o(\psi_o - \bar{\psi}), \tag{6}$$

where ψ_i and ψ_o are the gravitational potential at the inner-core and core-mantle boundaries, and $\bar{\psi}$ is the mass-averaged gravitational potential in the outer core[120]. Equation (6) shows that the convective power originates from taking mass anomalies at the gravitational potential of the inner or outer boundary, and redistributing it throughout the outer core at the mean gravitational potential.

Expressions (3)-(6) contain several approximations[120,121], including the assumption of a well-mixed core. The errors associated with these approximations are comparable to that of the Boussinesq approximation, which is $\sim 10\% - 15\%$. More precise expressions[27,28,125–127] lead to conclusions similar to those drawn below.

The inner-core growth rate $\dot{r}_i$, and consequently the convective forcing F_i at the inner-core boundary, do not depend on the thermal conductivity (equations 5 and 4). When the inner core is growing, the convective power $\Phi_{\rm conv}$ (equation 6) therefore remains large regardless of the value of k. Even with a high thermal conductivity $k > 100$ W m^{-1} K^{-1}, the convective power is larger than 1 TW at present (dotted lines at time 0 Gyr in Figure 4a,b). With a core heat flow $Q_{\rm cmb} = 10$ TW, the available convective power is 1.5 TW with $k = 100$ W m^{-1} K^{-1} and 2.5 TW with $k = 40$ W m^{-1} K^{-1} (time 0 Gyr in figure 4b). The power raises up to $3-4$ TW when assuming a large heat flow of 15 TW escaping from the core (time 0 Gyr in figure 4a).

4.3 The new core paradox

Trouble comes prior to the onset of inner-core growth. At the present day, the contribution F_i (equations 4) from the solidification of the inner core represents more than 70% of the mass anomaly flux that drives convection. Before the nucleation of the inner core, the major power contributor to the current geodynamo was therefore missing. The only power source that remained was thermal convection due to the slow cooling of the core. The core heat flow must then exceed the conducted heat flow to drive convection, as shown by expressions (3) and (6). However, the core heat flow ranges within $6-17$ TW[128–132] while the conducted heat flow is larger than 15 TW when the thermal conductivity is larger than 100 W m^{-1} K^{-1}. The heat budget of the core is hence very tight when $k \gtrsim 100$ W m^{-1} K^{-1}. This serious problem was termed the *new core paradox*[17] as it comes after

the Higgins-Kennedy core paradox raised and solved in the 1970s[133,134]. The growth of the inner core likely started less than 1 Gyr ago[27,28,125,132]. The new core paradox therefore impacts more than 2.4 Gyrs, hence 70% of the observed history of Earth's magnetic field.

The convective power $\Phi_{\rm conv}$ must necessarily be positive to sustain a convective dynamo. More stringent requirements are obtained from paleointensity measurements[61] (figure 2d) combined with scaling laws from dynamo simulations[84] (details in Supplementary Note 1). These require the ohmic dissipation, and hence the convective power $\Phi_{\rm conv}$, to be in the range $0.1-10$ TW over Earth's history (shaded region in figure 4a,b). Another condition is that the convective velocity U must be large enough so that the magnetic Reynolds number $Rm = U\,D/\eta$ (box 1) exceeds about 100 [83], where η is the magnetic diffusivity of the core and D the outer core thickness.

Prescribing the time-evolution of the core heat flow $Q_{\rm cmb}(t)$ and the radiogenic heating term $Q_r(t)$, one can integrate equations (3)-(6) backward in time to estimate the convective power in the past. Here, it is assumed that $Q_{\rm cmb}(t)$ increases linearly in the past, and that $Q_r = 0$ at all times. With the evolution of the convective power, dynamo scaling laws[12,135] are used to estimate the convective velocity U, and hence the magnetic Reynolds number Rm. Figure 4 shows the convective power and the magnetic Reynolds number from this evolutionary model.

Assuming a low thermal conductivity $k = 40\ \mathrm{W\,m^{-1}\,K^{-1}}$, convection can easily provide a power larger than 0.1 TW and a magnetic Reynolds number $Rm > 100$ during the last 4 billion years (dashed lines in figure 4).

In contrast, with a high conductivity of $100\ \mathrm{W\,m^{-1}\,K^{-1}}$, the convective power and Rm match the above constraints only when the present-day core heat flow $Q_{\rm cmb} \gtrsim 15$ TW (dotted lines in figure 4). This value is close to the upper estimates of the present-day $Q_{\rm cmb}$[130,136]. A thermal conductivity larger than $100\ \mathrm{W\,m^{-1}\,K^{-1}}$ therefore precludes an ancient dynamo driven by thermal convection. These results prompt the study of auxiliary sources of power.

4.4 The exsolution boost

Exsolution of light elements can contribute to core convection and the geodynamo[88,89,137]. When exsolution takes place near the CMB, exsolution releases a denser liquid with a mass anomaly flux[31,89]

$$F_{ex} \simeq -\alpha_c\, M_c\, \frac{\mathrm{d}C}{\mathrm{d}T}\,\frac{\mathrm{d}T_{\rm cmb}}{\mathrm{d}t}, \tag{7}$$

where $\alpha_c = -\left(\partial\rho/\partial C\right)/\rho$ is the chemical expansion coefficient for a given light element, C the concentration of this element in the liquid core measured by the total mass of the light element divided by the outer core mass M_c, and $T_{\rm cmb}$ is the CMB temperature. While the value of the chemical expansion coefficient α_c is close to one for both MgO and SiO_2[89,137,138], values of the exsolution rate $\mathrm{d}C/\mathrm{d}T$ are debated. For MgO, high-pressure experiments[88,139] find rates of $0.2-0.6\times10^{-5}\ \mathrm{K^{-1}}$ while molecular dynamics simulations[93] suggest rates 10 times larger. For SiO_2, experiments[89] suggest a high exsolution rate of $4\times10^{-5}\mathrm{K^{-1}}$.

The exsolution rate of light elements in the core affects the power available for the dynamo, expressed as

$$\Phi_{\rm conv} = (F_o + F_{ex})(\psi_o - \bar{\psi}) \tag{8}$$

before the birth of the inner core. Using the exsolution rates from experiments[88,89,139], MgO-exsolution generates an added power of about 0.5 TW while SiO_2-exsolution yields an added power of about 3 TW (Supplementary Figure 2). When it is coupled with thermal convection, exsolution substantially helps driving the dynamo[88,138].

However, to solve the new core paradox, exsolution must also loosen the restrictions on the thermal conductivity. Thermal convection alone can drive a dynamo with no inner core only when the thermal conductivity $k \lesssim 100\ \mathrm{W\,m^{-1}K^{-1}}$. With the help of MgO-exsolution at a rate of $0.5\times10^{-5}\ \mathrm{K^{-1}}$, the conductivity range widens only moderately to $k \lesssim 130\ \mathrm{W\,m^{-1}K^{-1}}$ (Supplementary Figure 3b). MgO-exsolution can drive a dynamo when the core is thermally stratified ($F_o < 0$ in (8)), but only for a narrow range of core heat flow[139] (Supplementary Figure 2 and 3a). The heat budget of the core therefore remains tight when using the low exsolution rate proposed for MgO[139,140].

In contrast, with the larger exsolution rate of $4\times10^{-5}\ \mathrm{K^{-1}}$ proposed for SiO_2[89], a thermal conductivity up to $k \simeq 350\ \mathrm{W\,m^{-1}K^{-1}}$ and a core heat flow as low as $Q_{\rm cmb} = 5$ TW are compatible with a long-lived geodynamo (Supplementary Figures 2 & 3ab). Such a high exsolution rate would solve the new core paradox.

4.5 Coupling with Earth's mantle

The heat flow $Q_{\rm cmb}$ escaping from the core enters the heat budget of the mantle, which reads[141,142]:

$$Q_{\rm surf} = Q_{\rm cmb} + H_{\rm m} - C_m\,\frac{\mathrm{d}T_{\rm m}}{\mathrm{d}t}, \tag{9}$$

where $Q_{\rm surf}$ is the heat flow at Earth's surface, $H_{\rm m}$ is the internal heat produced by radiogenic elements in the mantle, C_m is the heat capacity of the mantle, and $T_{\rm m}$ its average temperature. The thermal evolution of the core is therefore coupled with that of the mantle[126,127].

At present, $Q_{\rm surf} \simeq 46$ TW while geochemical models[67] imply $H_{\rm m} \simeq 18$ TW. The difference must be balanced by the mantle cooling and the heat $Q_{\rm cmb}$ escaping from the core in equation (9). For $Q_{\rm cmb} < 10$ TW, thermal evolution models[142] predict a cooling rate of more than $200\,{\rm K\,Gyr^{-1}}$, three times larger than estimated from petrological observations[143,144], implying massive melting of the mantle as recently as 2 Gyrs ago. This conundrum is known as the mantle thermal catastrophe.

The large $Q_{\rm cmb}$ values needed to sustain the geodynamo at ancient times therefore help in avoiding the mantle thermal catastrophe[126,127].

However, a high core heat flow also implies a fast cooling rate of the core, and hence can lead to a core thermal catastrophe with a temperature exceeding 5500K below the core-mantle boundary 3 Gyrs ago[27]. With such high core temperatures, the lower mantle was molten, forming a basal magma ocean[145]. This scenario of a hot early core and a basal magma ocean is acceptable as long as the upper mantle remains solid for the last 3.5 Gyrs.

Some proposed that convection in the basal magma ocean could generate Earth's magnetic field in the early Earth[146–148]. Using an electrical conductivity of 2×10^4 S m^{-1} [147] and the same dynamo scaling as in figure 4cd, with a convective power of ~ 1 TW in a 300 km thick ocean[148], yields a magnetic Reynolds number $Rm \approx 12$. Such a value of the magnetic Reynolds number is too small to drive dynamo action (box 1). In addition, it remains uncertain whether the basal ocean convects or is chemically stratified[149].

5 Sustaining a mechanical geodynamo

The new core paradox motivates the assessment of precession or tides as alternative driving mechanisms[44,101,103]. In this section, the orbital history of the Earth-Moon system is combined with the latest results on the flows driven by precession and tides to determine whether these mechanisms could have powered the ancient geodynamo.

5.1 An elusive power estimate

Precession and tides tap into the rotational and gravitational energy reservoir stored into the spinning Earth and its orbiting Moon, of which 10^{29} J are left today[101]. In contrast with the convective case, the orbital power that is converted into turbulent flows and available to the dynamo is much harder to estimate.

Still, an upper bound can be obtained from orbital observations, which are the recession of the Moon and the increase in Earth's length-of-day. The total dissipation of the Earth-Moon system $\Phi_{\rm orb}$ varies from 1 TW to 15 TW during Earth's history, with an average value of 2 to 3 TW (Supplementary Figure 4). Current models assume that this power is dissipated in ocean tides through Earth's history[150]. Yet, a fraction of this dissipation could have occurred in the Earth's core. Today, for a total tidal dissipation of 2.2 TW about 0.1 TW is dissipated in the core and mantle[151]. The fraction dissipated in the core could have been larger in the past when the Moon was closer to the Earth. The total dissipated power $\Phi_{\rm orb}$ can be seen as the analogue for the total heat flow out of the Earth, from which only a small fraction might contribute to the geodynamo. This upper bound is larger than the minimum power of 0.1 TW needed to drive the ancient geodynamo (section 4.3). Thus, the orbital history of the Earth-Moon system leaves room for an orbitally-driven dynamo in the past, but not with an ample margin.

Whether the flow excited by precession or tides can convert part of this power into the geomagnetic field is an unsettled question. The power drawn by laminar[34,35] and turbulent[105] flows due to the strong shear at the boundaries is at least two orders of magnitude too low to feed the ohmic dissipation of the geodynamo. These conclusions do not change when including the dissipation in the boundary layer near the inner core, or by considering a CMB topography < 10 km (details in Supplementary Note 2).

Flow instabilities and turbulence in the bulk core could drain notably more power from Earth's orbital evolution, with a theoretical upper bound for the dissipation[152] of 10^9 TW. This value implies that the total energy of 10^{29} J contained in the Earth-Moon would be dissipated in a few years. This upper bound is therefore too large to be useful.

The above arguments demonstrate that turbulence in the bulk core is a necessary condition to sustain an orbitally-driven geodynamo. In the following section, we examine whether turbulent bulk flows can be triggered by precession and tides in Earth's core and whether they are strong enough to produce a dynamo.

5.2 Turbulence in the bulk core

Bulk turbulence requires the laminar flow to be unstable, which happens when the strain rate is larger than the viscous damping rate, that is

$$\xi u f > K\sqrt{\nu\Omega}, \tag{10}$$

where ν is the kinematic viscosity, Ω the Earth's rotation rate, $K \gtrsim 2.62$ a damping coefficient[36,153], ξ a numerical prefactor ($\xi \lesssim 9/16$ for tides[154], and $\xi \lesssim 5\sqrt{15}/32$ for precession[153]). For precession, $u = u_p$ is the differential velocity between the outer core and the mantle and $f = f_p$ the polar ellipticity. For tides, $u = u_t$ is the speed of the tidal bulge at the CMB as it rotates around the core and $f = f_t$ the diurnal tidal ellipticity.

While a convective geodynamo highly depends on the value of core thermal conductivity (section 4.3), condition (10) shows that core viscosity is the key parameter for a dynamo driven by precession or tides. The current Earth's core is marginally stable to bulk instabilities for both precession[103,153,155] and tides[156]. Whether turbulent bulk flows can develop is therefore very sensitive to the value of core viscosity, estimates of which range from[157] 3×10^{-7} to 5×10^{-6} m^2/s.

Using the most accepted scenario for the evolution of orbital parameters over time[158,159] yields a past obliquity lower than the current 23.5° value (orange curve in figure 5a). With this scenario, precession meets condition (10) only for a low viscosity of $\nu \sim 10^{-7}$ m^2 s^{-1} and prior to 3 Gyrs ago (figure 5a). Even in the high-obliquity scenario, a viscosity of $\nu = 10^{-6}$ m^2 s^{-1} is not low enough for instabilities to grow (Supplementary Figures 5). Core-filling turbulence driven by precession is therefore unlikely in Earth's core.

Because the Earth and Moon were closer in the past, the diurnal tidal ellipticity increases when going back in time (orange curve in figure 5b). With this evolution, tides can easily meet condition (10). With a viscosity of 10^{-6} m^2 s^{-1} or 3×10^{-6} m^2 s^{-1}, tidal instabilities occur prior to 1.5 Gyrs or 3 Gyrs ago, respectively.

The growth of instabilities is not the only condition to power a dynamo. In addition, the vigour of the bulk flow, as measured by the magnetic Reynolds number Rm, must be high enough (box 1). Results obtained for tides, both experimentally[160] and numerically[161], suggest that inertial instabilities can sustain a turbulent flow of the order uf. From this scaling for the vigour of bulk flows, and criterion (10) for their emergence, the evolution of orbital parameters over time[158,159] (detailed in Supplementary Note 2) allows to estimate the magnetic Reynolds number Rm for precession-driven and tidal flows (figure 5 and Supplementary Figure 5). Bulk flows driven by precession yield $Rm \lesssim 60$ at all times (fig. 5a), which is hardly enough for a dynamo. In contrast, $Rm \gtrsim 100$ for the tidal flow in the core, reaching $Rm \simeq 700$ for the early Earth (figure 5b).

Thus, even in the unlikely event that precession triggers bulk instabilities, the resulting flows are not strong enough to generate a magnetic field. In contrast, tides can excite strong flows filling the entire core. These could drive a dynamo, especially in the early stages of Earth's history.

6 Implications

The long-term evolution of the geodynamo is inherently connected with the thermal history of the core and mantle, the evolution of stratified layers in the core and the observed paleomagnetic field.

6.1 Thermal history of the core and mantle

With a high or moderate thermal conductivity, the current core heat flow Q_{cmb} must exceed ~ 10 TW to drive a convective geodynamo. Such a high core heat flow is compatible with global mantle convection models[132] and could avert the mantle thermal catastrophe[126,127] (equation (9)).

Only a few investigations couple the thermal evolution of the core and mantle. They solve simultaneously the energy budget for both layers[126,127,137]. When the lower mantle is about 5 times more viscous than the upper mantle, these models produce a current CMB heat flow of about 13 TW, which reaches up to $40-80$ TW in the distant past. These values allow for a long-lived convective dynamo while avoiding the mantle thermal catastrophe[126,127]. A current CMB heat flow larger than 13 TW implies that the inner core is less than 700 million year old and that the lower mantle was molten before 2 ± 1 Gyr ago[27,28].

It has been hypothesized that the core is cooling too slowly to power a convective dynamo[44]. This scenario relies on the early mantle be fully molten. A fully-molten mantle would cool down the core in less than 100 Myrs and hence would leave no heat to drive the geodynamo by convection during the subsequent billion years[162]. However, it is plausible that only a fraction of Earth's mantle was molten during the last giant impact that formed the Earth[91]. With a partially-solid, hence viscous, mantle above it, the core likely retained enough heat to power a convective dynamo.

6.2 Stratification in the early core

During the accretion of the Earth, giant impacts brought metal into contact with liquid silicates at very high temperature, facilitating the dissolution of light elements into the core[30,31,72,87,163]. The metal added by each giant impact was enriched in light elements[164] and hence formed stratified layers at the top of the core[165]. The mixing during a giant impact was too small to destroy this stratification[166,167]. The early core was therefore likely stratified in composition over hundreds of kilometers, with a stratification strength, as measured by the buoyancy frequency N, 2 to 10 times the Earth's rotation rate Ω[165–167].

Such a strong stratification would prevent the generation of magnetic fields by tides[168]. Similarly, convection would have a hard time to overcome this stratification unless the latter is localised at the top or bottom of the core.

Geodynamo simulations indicate that, at the present day, the stratified layer atop Earth's core must be thinner than about $100-300$ km with a stratification not stronger than $N \sim \Omega$ to be compatible with geomagnetic observations[169–171]. A mechanism therefore destroyed or partially mixed the primordial stratification. Yet, numerical simulations[167] suggest that thermal convection cannot erode more than 10 km of primordial stratification. Tidal flows or chemical convection due to the exsolution of light elements are possible mixing mechanisms that deserve further studies.

6.3 Paleomagnetic field

The driving mechanism of the geodynamo controls the strength and morphology of the paleomagnetic field. Paleomagnetic data hence provide clues about the dynamo mechanism and its evolution through time[61,63,64,70].

The nucleation of the inner core was a major transition for the dynamo mechanism. In the presence of a growing inner core, a light fluid is released at the inner-core boundary and drives convection (section 4.2). This driving mechanism was missing prior to the growth of an inner core (section 4.3), irrespective of whether tides or convection drove the ancient dynamo. The nucleation of the inner-core therefore coincided with a strong increase in the power available to the dynamo (section 4.3).

Theory has long predicted that this increase in power left footprints in the paleointensity record[70,141]. However, paleointensity does not vary substantially over Earth's history[61] (figure 2d). Dynamo simulations linked with thermal evolution of the core allow to investigate the signature of inner-core growth on a convective geodynamo[97,98]. Such simulations suggest that the nucleation of the inner core caused an increase in magnetic field strength inside the core, but no resolvable change in the field intensity at Earth's surface[97]. This result reconciles the absence of long-term trends in the paleointensity record with theoretical predictions. It also suggests that long-term paleointensity trends are unlikely to constrain the age of the inner core.

Still, these evolutionary dynamo simulations indicate that, during short time intervals, the magnetic field can be weak and multipolar prior to inner-core growth[97,98]. A multipolar field could have caused short-lasting paleomagnetic anomalies. Such anomalies have been reported in the paleomagnetic record[172,173] for ages ~ 375 Ma and ~ 580 Ma. Further paleomagnetic investigations are needed to know whether these anomalies could be a signature of the absence of an inner core.

A geodynamo driven by convection is therefore compatible with paleomagnetic data. However, only a few dynamo simulations with no inner core have been published[84,96,97]. More simulations, especially in a turbulent regime, are needed to better understand the ancient geodynamo and its paleomagnetic signature.

7 Summary and future directions

Unlike mechanical dynamos, a geodynamo driven by thermo-chemical convection accounts for most of the properties of the geomagnetic field (table in box 2). Convection also produces enough power to generate a magnetic field over the last 3.4 Gyrs, as inferred from paleomagnetic data. Convection therefore remains the most likely driving mechanism for the geodynamo.

Yet, convective dynamo models almost all assume that composition and temperature have the same diffusivity, while light elements released at the inner-core boundary diffuse several orders of magnitude slower than temperature. The effect of double diffusion, when temperature and composition diffuse at different rates, on the geodynamo has been little studied[174–178]. Further examination of double diffusion could open new avenues for exploring the dynamics of Earth's core.

Whether the exsolution of light elements solves the new core paradox strongly depends on the value of the exsolution rate, which is debated[88,89,93,139]. More precise estimates of the exsolution rate from high-pressure experiments and calculations are therefore needed. In addition, whether MgO[88,139], or SiO2[89], or other components[94,138] exsolve, and when their exsolution started, is an unsettled issue. It remains unknown whether the early core contained sufficient amounts of magnesium for the exsolution mechanism to start prior to 3 Gyrs ago and power the early geodynamo[94,138,179]. Similarly, SiO_2 might not start exsolving at temperatures larger than 4000 K[179], which are expected in the ancient core. Oxides are extracted from the core at a rate set by mantle convection[138]. This interaction with the mantle notably affects the nature of the exsolved species and the time at which exsolution starts[138], and therefore deserves further investigation.

In the Earth's core, precession requires an unlikely low viscosity to trigger bulk turbulence together with an unlikely high obliquity (figure 5a and Supplementary Figure 5). Even under such favourable circumstances, the predicted flow velocity is hardly sufficient for magnetic induction to overcome ohmic dissipation (figure 5a). In addition, the magnetic field obtained in precession-driven dynamos does not match the properties of the modern geomagnetic field (figure 3d and table in box 2).

Unlike precession, tides can generate vigourous bulk flows in the early Earth. However, the flows and magnetic fields driven by tides are poorly known. Numerical simulations of tide-driven dynamos are in their infancy in deformed spheres, with a single proof-of-concept kinematic dynamo[106]. A dynamo driven by tides in the past would require a substantial fraction of the power currently attributed to the oceans[150] to be dissipated in the core.

References

1. Lundin, R., Lammer, H. & Ribas, I. Planetary magnetic fields and solar forcing: implications for atmospheric evolution. *Space Sci. Rev.* **129**, 245–278 (2007).

2. Lammer, H. *et al.* Coronal mass ejection (CME) activity of low mass m stars as an important factor for the habitability of terrestrial exoplanets. II. CME-induced ion pick up of earth-like exoplanets in close-in habitable zones. *Astrobiology* **7**, 185–207 (2007).

3. Gunell, H. *et al.* Why an intrinsic magnetic field does not protect a planet against atmospheric escape. *Astron. & Astrophys.* **614**, L3 (2018).

4. Lohmann, K., Putman, N. & Lohmann, C. Geomagnetic imprinting: A unifying hypothesis of long-distance natal homing in salmon and sea turtles. *Proc. Natl. Acad. Sci.* **105**, 19096–19101 (2008).

5. Benhamou, S. *et al.* The role of geomagnetic cues in green turtle open sea navigation. *PloS one* **6**, e26672 (2011).

6. Rismani Yazdi, S. *et al.* Magnetotaxis: Magnetotaxis enables magnetotactic bacteria to navigate in flow. *Small* **14**, 1870019 (2018).

7. Roque, B., Rosselli, A., Mitchell, C. & Petroff, A. Control of multicellular magnetotactic bacteria with a magnetic field. In *APS March Meeting Abstracts*, L70.321 (2019).

8. Larmor, J. How could a Rotating Body such as the Sun become a Magnet? *Report of the British Association for the Advancement of Science* **87th meeting**, 159–160 (1919).

9. Roberts, P. H. & King, E. M. On the genesis of the Earth's magnetism. *Reports on Prog. Phys.* **76**, 096801 (2013).

10. Christensen, U. R., Aubert, J. & Hulot, G. Conditions for Earth-like geodynamo models. *Earth Planet. Sci. Lett.* **296**, 487–496 (2010).

11. Schaeffer, N., Jault, D., Nataf, H.-C. & Fournier, A. Turbulent geodynamo simulations: a leap towards Earth's core. *Geophys. J. Int.* **211**, 1–29 (2017).

12. Aubert, J., Gastine, T. & Fournier, A. Spherical convective dynamos in the rapidly rotating asymptotic regime. *J. Fluid Mech.* **813**, 558–593 (2017).

13. Sheyko, A., Finlay, C., Favre, J. & Jackson, A. Scale separated low viscosity dynamos and dissipation within the Earth's core. *Sci. reports* **8**, 1–7 (2018).

14. Aubert, J. & Finlay, C. C. Geomagnetic jerks and rapid hydromagnetic waves focusing at Earth's core surface. *Nat. Geosci.* **12**, 393–398 (2019).

15. Aubert, J. & Gillet, N. The interplay of fast waves and slow convection in geodynamo simulations nearing Earth's core conditions. *Geophys. J. Int.* **225**, 1854–1873 (2021).

16. Tarduno, J. A. *et al.* Geodynamo, solar wind, and magnetopause 3.4 to 3.45 billion years ago. *Science* **327**, 1238–1240 (2010).

17. Olson, P. The new core paradox. *Science* **342**, 431–432 (2013).

18. Konôpková, Z., McWilliams, R. S., Gómez-Pérez, N. & Goncharov, A. F. Direct measurement of thermal conductivity in solid iron at planetary core conditions. *Nature* **534**, 99–101 (2016).

19. Hasegawa, A., Yagi, T. & Ohta, K. Combination of pulsed light heating thermoreflectance and laser-heated diamond anvil cell for in-situ high pressure-temperature thermal diffusivity measurements. *Rev. Sci. Instruments* **90**, 074901 (2019).

20. Hsieh, W.-P. *et al.* Low thermal conductivity of iron-silicon alloys at Earth's core conditions with implications for the geodynamo. *Nat. communications* **11**, 1–7 (2020).

21. Stacey, F. D. & Anderson, O. L. Electrical and thermal conductivities of Fe–Ni–Si alloy under core conditions. *Phys. Earth Planet. Int.* **124**, 153–162 (2001).

22. Stacey, F. D. & Loper, D. E. A revised estimate of the conductivity of iron alloy at high pressure and implications for the core energy balance. *Phys. Earth Planet. Int.* **161**, 13–18 (2007).

23. de Koker, N., Steinle-Neumann, G. & Vlček, V. Electrical resistivity and thermal conductivity of liquid Fe alloys at high P and T, and heat flux in Earth's core. *Proc. Natl. Acad. Sci.* **109**, 4070–4073 (2012).

24. Pozzo, M., Davies, C., Gubbins, D. & Alfè, D. Thermal and electrical conductivity of iron at Earth's core conditions. *Nature* **485**, 355–358 (2012).

25. Gomi, H. *et al.* The high conductivity of iron and thermal evolution of the earth's core. *Phys. Earth Planet. Int.* **224**, 88–103 (2013).

26. Ohta, K., Kuwayama, Y., Hirose, K., Shimizu, K. & Ohishi, Y. Experimental determination of the electrical resistivity of iron at Earth's core conditions. *Nature* **534**, 95–98 (2016).

27. Labrosse, S. Thermal evolution of the core with a high thermal conductivity. *Phys. Earth Planet. Int.* **247**, 36–55 (2015).

28. Davies, C. Cooling history of Earth's core with high thermal conductivity. *Phys. Earth Planet. Int.* **247**, 65–79 (2015).

29. Buffett, B. A., Garnero, E. J. & Jeanloz, R. Sediments at the top of Earth's core. *Science* **290**, 1338–1342 (2000).

30. Badro, J., Siebert, J. & Nimmo, F. An early geodynamo driven by exsolution of mantle components from Earth's core. *Nature* **536**, 326–328 (2016).

31. O'Rourke, J. & Stevenson, D. Powering Earth's dynamo with magnesium precipitation from the core. *Nature* **529**, 387–389 (2016).

32. Malkus, W. V. R. Precession of the Earth as the cause of geomagnetism. *Science* **160**, 259–264 (1968).

33. Stacey, F. The coupling of the core to the precession of the Earth. *Geophys. J. Int.* **33**, 47–55 (1973).

34. Loper, D. E. Torque balance and energy budget for the precessionally driven dynamo. *Phys. Earth Planet. Int.* **11**, 43–60 (1975).

35. Rochester, M. G., Jacobs, J. A., Smylie, D. E. & Chong, K. F. Can precession power the geomagnetic dynamo? *Geophys. J. Int.* **43**, 661–678 (1975).

36. Le Bars, M., Lacaze, L., Le Dizes, S., Le Gal, P. & Rieutord, M. Tidal instability in stellar and planetary binary systems. *Phys. Earth Planet. Int.* **178**, 48–55 (2010).

37. Grannan, A., Le Bars, M., Cébron, D. & Aurnou, J. Experimental study of global-scale turbulence in a librating ellipsoid. *Phys. Fluids* **26**, 126601 (2014).

38. Lin, Y., Noir, J. & Jackson, A. Experimental study of fluid flows in a precessing cylindrical annulus. *Phys. Fluids* **26**, 046604 (2014).

39. Lemasquerier, D. *et al.* Libration-driven flows in ellipsoidal shells. *J. Geophys. Res. Planets* **122**, 1926–1950 (2017).

40. Tilgner, A. Precession driven dynamos. *Phys. Fluids* **17**, 034104 (2005).

41. Wu, C.-C. & Roberts, P. H. On a dynamo driven topographically by longitudinal libration. *Geophys. Astrophys. Fluid Dyn.* **107**, 20–44 (2013).

42. Ernst-Hullermann, J., Harder, H. & Hansen, U. Finite volume simulations of dynamos in ellipsoidal planets. *Geophys. J. Int.* **195**, 1395–1405 (2013).

43. Lin, Y., Marti, P., Noir, J. & Jackson, A. Precession-driven dynamos in a full sphere and the role of large scale cyclonic vortices. *Phys. Fluids* **28**, 066601 (2016).

44. Andrault, D., Monteux, J., Le Bars, M. & Samuel, H. The deep Earth may not be cooling down. *Earth Planet. Sci. Lett.* **443**, 195–203 (2016).

45. Hulot, G., Olsen, N., Sabaka, T. J. & Fournier, A. The present and future geomagnetic field. In Kono, M. & Schubert, G. (eds.) *Geomagnetism*, vol. 5 of *Treatise on Geophysics*, chap. 2, 33–78 (Elsevier, Amsterdam, 2015), 2 edn.

46. Alken, P. *et al.* International Geomagnetic Reference Field: the 13th generation. *Earth, Planets Space* **73**, 49 (2021).

47. Olsen, N., Hulot, G. & Sabaka, T. J. Sources of the geomagnetic field and the modern data that enable their investigation. In Freeden, W., Nashed, M. Z. & Sonar, T. (eds.) *Handbook of Geomathematics*, 105–124 (Springer Berlin Heidelberg, 2010).

48. Jonkers, A. R. T., Jackson, A. & Murray, A. Four centuries of geomagnetic data from historical records. *Rev. Geophys.* **41**, 1006 (2003).

49. Jackson, A. & Finlay, C. C. Geomagnetic secular variation and its applications to the core. In Kono, M. & Schubert, G. (eds.) *Geomagnetism*, vol. 5 of *Treatise on Geophysics*, chap. 5, 137–184 (Elsevier, Amsterdam, 2015), 2 edn.

50. Gillet, N., Jault, D. & Finlay, C. C. Planetary gyre, time-dependent eddies, torsional waves, and equatorial jets at the Earth's core surface. *J. Geophys. Res. Solid Earth* **120**, 3991–4013 (2015).

51. Gillet, N., Jault, D., Canet, E. & Fournier, A. Fast torsional waves and strong magnetic field within the Earth's core. *Nature* **465**, 74–77 (2010).

52. Braginsky, S. I. & Roberts, P. H. Equations governing convection in Earth's core and the geodynamo. *Geophys. Astrophys. Fluid Dyn.* **79**, 1–97 (1995).

53. Holme, R. Large-scale flow in the core. In Olson, P. & Schubert, G. (eds.) *Core dynamics*, vol. 8 of *Treatise on Geophysics*, chap. 4, 91–113 (Elsevier, Oxford, 2015), 2 edn.

54. Channell, J. E. T., Kent, D. V., Lowrie, W. & Meert, J. G. *Timescales of the paleomagnetic field*, vol. 145 (American Geophysical Union, 2004).

55. Gallet, Y. *et al.* On the use of archeology in geomagnetism, and vice-versa: Recent developments in archeomagnetism. *Comptes Rendus Physique* **10**, 630–648 (2009).

56. Evans, D. A. D. Reconstructing pre-Pangean supercontinents. *GSA Bull.* **125**, 1735–1751 (2013).

57. Nichols, C. *et al.* Hints of an Eoarchean magnetic field from the Isua Supracrustal Belt, Greenland. *AGU* Abstract DI14A–02 (2019).

58. Tarduno, J., Cottrell, R., Davis, W., Nimmo, F. & Bono, R. A Hadean to Paleoarchean geodynamo recorded by single zircon crystals. *Science* **349**, 521–524 (2015).

59. Weiss, B. *et al.* Secondary magnetic inclusions in detrital zircons from the Jack Hills, western Australia, and implications for the origin of the geodynamo. *Geology* **46**, 427–430 (2018).

60. Olson, P., Deguen, R., Hinnov, L. & Zhong, S. Controls on geomagnetic reversals and core evolution by mantle convection in the Phanerozoic. *Phys. Earth Planet. Int.* **214**, 87–103 (2013).

61. Biggin, A. J. *et al.* Palaeomagnetic field intensity variations suggest Mesoproterozoic inner-core nucleation. *Nature* **526**, 245–248 (2015).

62. Smirnov, A. V., Tarduno, J. A., Kulakov, E. V., McEnroe, S. A. & Bono, R. K. Palaeointensity, core thermal conductivity and the unknown age of the inner core. *Geophys. J. Int.* **205**, 1190–1195 (2016).

63. Valet, J.-P., Besse, J., Kumar, A., Vadakke-Chanat, S. & Philippe, E. The intensity of the geomagnetic field from 2.4 Ga old Indian dykes. *Geochem. Geophys. Geosystems* **15**, 2426–2437 (2014).

64. Smirnov, A. V., Tarduno, J. A. & Evans, D. A. Evolving core conditions ca. 2 billion years ago detected by paleosecular variation. *Phys. Earth Planet. Int.* **187**, 225–231 (2011).

65. Evans, D. Proterozoic low orbital obliquity and axial-dipolar geomagnetic field from evaporite palaeolatitudes. *Nature* **444**, 51–55 (2006).

66. Jaupart, C., Labrosse, S., Lucazeau, F. & Mareschal, J.-C. Temperatures, heat, and energy in the mantle of the Earth. In Bercovici, D. & Schubert, G. (eds.) *Mantle Convection*, Treatise on Geophysics, chap. 6, 223 – 270 (Elsevier, Oxford, 2015), 2 edn.

67. McDonough, W. F. & Sun, S.-s. The composition of the Earth. *Chem. Geol.* **120**, 223–253 (1995).

68. Palme, H. & O'Neill, H. St. C. Cosmochemical estimates of mantle composition. In Holland, H. D. & Turekian, K. K. (eds.) *Treatise on Geochemistry*, 1–38 (Pergamon, Oxford, 2007).

69. Gubbins, D. Energetics of the Earth's core. *J. Geophys.* **43**, 453–464 (1977).

70. Olson, P. A simple physical model for the terrestrial dynamo. *J. Geophys. Res. Solid Earth* **86**, 10875–10882 (1981).

71. Loper, D. E. & Roberts, P. Compositional convection and the gravitationally powered dynamo. *Stellar planetary magnetism* 297–327 (1983).

72. Hirose, K., Wood, B. & Vočadlo, L. Light elements in the Earth's core. *Nat. Rev. Earth & Environ.* **2**, 645–658 (2021).

73. Bouffard, M., Choblet, G., Labrosse, S. & Wicht, J. Chemical convection and stratification in the Earth's outer core. *Front. Earth Sci.* **7**, 99 (2019).

74. Busse, F. H. Thermal instabilities in rapidly rotating systems. *J. Fluid. Mech.* **44**, 441–460 (1970).

75. Cardin, P. & Olson, P. An experimental approach to thermochemical convection in the Earth's core. *Geophys. research letters* **19**, 1995–1998 (1992).

76. Sumita, I. & Olson, P. Laboratory experiments on high Rayleigh number thermal convection in a rapidly rotating hemispherical shell. *Phys. Earth Planet. Int.* **117**, 153–170 (2000).

77. King, E. M., Stellmach, S., Noir, J., Hansen, U. & Aurnou, J. M. Boundary layer control of rotating convection systems. *Nature* **457**, 301–304 (2009).

78. Gastine, T., Wicht, J. & Aubert, J. Scaling regimes in spherical shell rotating convection. *J. Fluid Mech.* **808**, 690–732 (2016).

79. Busse, F. H. A model of the geodynamo. *Geophys. J. Royal Astron. Soc.* **42**, 437–459 (1975).

80. Glatzmaier, G. A. & Roberts, P. H. A three-dimensional self-consistent computer simulation of a geomagnetic field reversal. *Nature* **377**, 203–209 (1995).

81. Kageyama, A., Sato, T. & the Complexity Simulation Group. Computer simulation of a magnetohydrodynamic dynamo. II. *Phys. Plasmas* **2**, 1421–1431 (1995).

82. Christensen, U. R. & Wicht, J. Numerical dynamo simulations. In Olson, P. & Schubert, G. (eds.) *Core dynamics*, Treatise on Geophysics, chap. 10, 245–277 (Elsevier, Oxford, 2015), 2 edn.

83. Christensen, U. & Aubert, J. Scaling properties of convection-driven dynamos in rotating spherical shells and application to planetary magnetic fields. *Geophys. J. Int.* **166**, 97–114 (2006).

84. Aubert, J., Labrosse, S. & Poitou, C. Modelling the palaeo-evolution of the geodynamo. *Geophys. J. Int.* **179**, 1414–1428 (2009).

85. Schwaiger, T., Gastine, T. & Aubert, J. Force balance in numerical geodynamo simulations: a systematic study. *Geophys. J. Int.* **219**, S101–S114 (2019).

86. Hori, K., Teed, R. J. & Jones, C. A. The dynamics of magnetic rossby waves in spherical dynamo simulations: a signature of strong-field dynamos? *Phys. Earth Planet. Int.* **276**, 68–85 (2018).

87. Fischer, R. A. *et al.* High pressure metal–silicate partitioning of Ni, Co, V, Cr, Si, and O. *Geochimica et Cosmochimica Acta* **167**, 177–194 (2015).

88. Badro, J. *et al.* Magnesium partitioning between Earth's mantle and core and its potential to drive an early exsolution geodynamo. *Geophys. Res. Lett.* **45**, 13,240–13,248 (2018).

89. Hirose, K. *et al.* Crystallization of silicon dioxide and compositional evolution of the Earth's core. *Nature* **543**, 99–102 (2017).

90. Nakajima, M. & Stevenson, D. J. Melting and mixing states of the Earth's mantle after the Moon-forming impact. *Earth Planet. Sci. Lett.* **427**, 286–295 (2015).

91. Nakajima, M. *et al.* Scaling laws for the geometry of an impact-induced magma ocean. *Earth Planet. Sci. Lett.* **568**, doi: 10.1016/j.epsl.2021.116983 (2021).

92. Huang, D., Badro, J., Brodholt, J. & Li, Y. Ab initio molecular dynamics investigation of molten Fe–Si–O in Earth's core. *Geophys. Res. Lett.* **46**, 6397–6405 (2019).

93. Liu, W., Zhang, Y., Yin, Q.-Z., Zhao, Y. & Zhang, Z. Magnesium partitioning between silicate melt and liquid iron using first-principles molecular dynamics: Implications for the early thermal history of the Earth's core. *Earth Planet. Sci. Lett.* **531**, 115934 (2020).

94. Helffrich, G., Hirose, K. & Nomura, R. Thermodynamical modeling of liquid Fe-Si-Mg-O: Molten magnesium silicate release from the core. *Geophys. Res. Lett.* **47**, e2020GL089218 (2020).

95. Arveson, S., Deng, J., Karki, B. & Lee, K. Evidence for Fe-Si-O liquid immiscibility at deep Earth pressures. *Proc. Natl. Acad. Sci.* **116**, 10238–10243 (2019).

96. Landeau, M. & Aubert, J. Equatorially asymmetric convection inducing a hemispherical magnetic field in rotating spheres and implications for the past martian dynamo. *Phys. Earth Planet. Int.* **185**, 61–73 (2011).

97. Landeau, M., Aubert, J. & Olson, P. The signature of inner-core nucleation on the geodynamo. *Earth Planet. Sci. Lett.* **465**, 193–204 (2017).

98. Driscoll, P. E. Simulating 2 Ga of geodynamo history. *Geophys. Res. Lett.* **43**, 5680–5687 (2016).

99. Busse, F. H. Steady fluid flow in a precessing spheroidal shell. *J. Fluid Mech.* **33**, 739–751 (1968).

100. Noir, J., Jault, D. & Cardin, P. Numerical study of the motions within a slowly precessing sphere at low Ekman number. *J. Fluid Mech.* **437**, 283–299 (2001).

101. Le Bars, M., Cébron, D. & Le Gal, P. Flows driven by libration, precession, and tides. *Annu. Rev. Fluid Mech.* **47**, 163–193 (2015).

102. Noir, J. & Cébron, D. Precession-driven flows in non-axisymmetric ellipsoids. *J. Fluid Mech.* **737**, 412–439 (2013).

103. Tilgner, A. Rotational dynamics of the core. In Olson, P. & Schubert, G. (eds.) *Core dynamics*, vol. 8 of *Treatise on Geophysics*, chap. 7, 183–212 (Elsevier, Oxford, 2015), 2 edn.

104. Tilgner, A. On models of precession driven core flow. *Studia geophysica et geodaetica* **42**, 232–238 (1998).

105. Cébron, D., Laguerre, R., Noir, J. & Schaeffer, N. Precessing spherical shells: flows, dissipation, dynamo and the lunar core. *Geophys. J. Int.* **219**, S34–S57 (2019).

106. Reddy, K. S., Favier, B. & Le Bars, M. Turbulent kinematic dynamos in ellipsoids driven by mechanical forcing. *Geophys. Res. Lett.* **45**, 1741–1750 (2018).

107. Wu, C.-C. & Roberts, P. H. On a dynamo driven by topographic precession. *Geophys. Astrophys. Fluid Dyn.* **103**, 467–501 (2009).

108. Guermond, J.-L., Léorat, J., Luddens, F. & Nore, C. Remarks on the stability of the Navier–Stokes equations supplemented with stress boundary conditions. *Eur. J. Mech.* **39**, 1–10 (2013).

109. Spence, E., Nornberg, M., Jacobson, C., Kendrick, R. & Forest, C. Observation of a turbulence-induced large scale magnetic field. *Phys. Rev. Lett.* **96**, 055002 (2006).

110. Monchaux, R. *et al.* Generation of a magnetic field by dynamo action in a turbulent flow of liquid sodium. *Phys. Rev. Lett.* **98**, 044502 (2007).

111. Zimmerman, D. S., Triana, S. A., Nataf, H.-C. & Lathrop, D. P. A turbulent, high magnetic Reynolds number experimental model of Earth's core. *J. Geophys. Res. Solid Earth* **119**, 4538–4557 (2014).

112. Cabanes, S., Schaeffer, N. & Nataf, H.-C. Turbulence reduces magnetic diffusivity in a liquid sodium experiment. *Phys. Rev. Lett.* **113**, 184501 (2014).

113. Stefani, F. *et al.* Towards a precession driven dynamo experiment. *Magnetohydrodynamics* **51**, 275–284 (2015).

114. Poirier, J.-P. *Introduction to the Physics of the Earth's Interior* (Cambridge University Press, 2000).

115. Williams, Q. The thermal conductivity of Earth's core: A key geophysical parameter's constraints and uncertainties. *Annu. Rev. Earth Planet. Sci.* **46**, 47–66 (2018).

116. Zhang, Y. *et al.* Reconciliation of experiments and theory on transport properties of iron and the geodynamo. *Phys. Rev. Lett.* **125**, 078501 (2020).

117. Pourovskii, L. V., Mravlje, J., Georges, A., Simak, S. I. & Abrikosov, I. A. Electron–electron scattering and thermal conductivity of iron at Earth's core conditions. *New J. Phys.* **19**, 073022 (2017).

118. Christensen, U. R. & Tilgner, A. Power requirement of the geodynamo from ohmic losses in numerical and laboratory dynamos. *Nature* **429**, 169–171 (2004).

119. Christensen, U. R. Dynamo scaling laws and applications to the planets. *Space Sci. Rev.* **152**, 565–590 (2010).

120. Buffett, B. A., Huppert, H. E., Lister, J. R. & Woods, A. W. On the thermal evolution of the Earth's core. *J. Geophys. Res.* **101**, 7989–8006 (1996).

121. Lister, J. R. Expressions for the dissipation driven by convection in the Earth's core. *Phys. Earth Planet. Int.* **140**, 145–158 (2003).

122. Gubbins, D., Alfè, D., Masters, G., Price, G. D. & Gillan, M. J. Can the Earth's dynamo run on heat alone? *Geophys. J. Int.* **155**, 609–622 (2003).

123. Gubbins, D., Alfè, D., Masters, G., Price, G. D. & Gillan, M. Gross thermodynamics of two-component core convection. *Geophys. J. Int.* **157**, 1407–1414 (2004).

124. Labrosse, S. Thermal and magnetic evolution of the Earth's core. *Phys. Earth Planet. Int.* **140**, 127–143 (2003).

125. Nimmo, F. Energetics of the core. In Olson, P. & Schubert, G. (eds.) *Core dynamics*, vol. 8 of *Treatise on Geophysics*, chap. 2, 27–55 (Elsevier, Oxford, 2015), 2 edn.

126. Driscoll, P. & Bercovici, D. On the thermal and magnetic histories of Earth and Venus: Influences of melting, radioactivity, and conductivity. *Phys. Earth Planet. Int.* **236**, 36–51 (2014).

127. Patočka, V., Šrámek, O. & Tosi, N. Minimum heat flow from the core and thermal evolution of the Earth. *Phys. Earth Planet. Int.* **305**, 106457 (2020).

128. Hernlund, J. W., Thomas, C. & Tackley, P. J. Phase boundary double crossing and the structure of Earth's deep mantle. *Nature* **434**, 882–886 (2005).

129. Buffett, B. The thermal state of the Earth's core. *Science* **299**, 1675–1676 (2003).

130. Lay, T., Hernlund, J. & Buffett, B. A. Core-mantle boundary heat flow. *Nat. Geosci.* **1**, 25–32 (2008).

131. Leng, W. & Zhong, S. Controls on plume heat flux and plume excess temperature. *J. Geophys. Res. Solid Earth* **113** (2008).

132. Olson, P., Deguen, R., Rudolph, M. L. & Zhong, S. Core evolution driven by mantle global circulation. *Phys. Earth Planet. Int.* **243**, 44–55 (2015).

133. Kennedy, G. C. & Higgins, G. H. The core paradox. *J. Geophys. Res.* **78**, 900–904 (1973).

134. Busse, F. Higgins-Kennedy paradox. In Gubbins, D. & Herrero-Bervera, E. (eds.) *Encyclopedia of geomagnetism and paleomagnetism*, 401–402 (2007).

135. Davidson, P. A. Scaling laws for planetary dynamos. *Geophys. J. Int.* **195**, 67–74 (2013).

136. Lay, T., Hernlund, J., Garnero, E. J. & Thorne, M. S. A post-perovskite lens and D" heat flux beneath the central Pacific. *Science* **314**, 1272–1276 (2006).

137. O'Rourke, J., Korenaga, J. & Stevenson, D. Thermal evolution of Earth with magnesium precipitation in the core. *Earth Planet. Sci. Lett.* **458**, 263–272 (2017).

138. Mittal, T. *et al.* Precipitation of multiple light elements to power Earth's early dynamo. *Earth Planet. Sci. Lett.* **532**, 116030 (2020).

139. Du, Z., Boujibar, A., Driscoll, P. & Fei, Y. Experimental constraints on an MgO exsolution-driven geodynamo. *Geophys. Res. Lett.* **46**, 7379–7385 (2019).

140. Olson, P., Landeau, M. & Hirsh, B. Laboratory experiments on rain-driven convection: Implications for planetary dynamos. *Earth Planet. Sci. Lett.* **457**, 403–411 (2017).

141. Stevenson, D. J., Spohn, T. & Schubert, G. Magnetism and thermal evolution of the terrestrial planets. *Icarus* **54**, 466–489 (1983).

142. Korenaga, J. Urey ratio and the structure and evolution of Earth's mantle. *Rev. Geophys.* **46** (2008).

143. Grove, T. & Parman, S. Thermal evolution of the Earth as recorded by komatiites. *Earth Planet. Sci. Lett.* **219**, 173–187 (2004).

144. Herzberg, C., Condie, K. & Korenaga, J. Thermal history of the Earth and its petrological expression. *Earth Planet. Sci. Lett.* **292**, 79–88 (2010).

145. Labrosse, S., Hernlund, J. W. & Coltice, N. A crystallizing dense magma ocean at the base of the Earth's mantle. *Nature* **450**, 866–869 (2007).

146. Ziegler, L. & Stegman, D. Implications of a long-lived basal magma ocean in generating Earth's ancient magnetic field. *Geochem. Geophys. Geosystems* **14**, 4735–4742 (2013).

147. Stixrude, L., Scipioni, R. & Desjarlais, M. P. A silicate dynamo in the early Earth. *Nat. communications* **11**, 1–5 (2020).

148. Blanc, N. A., Stegman, D. R. & Ziegler, L. B. Thermal and magnetic evolution of a crystallizing basal magma ocean in Earth's mantle. *Earth Planet. Sci. Lett.* **534**, 116085 (2020).

149. Laneuville, M., Hernlund, J., Labrosse, S. & Guttenberg, N. Crystallization of a compositionally stratified basal magma ocean. *Phys. Earth Planet. Int.* **276**, 86–92 (2018).

150. Tyler, R. H. On the tidal history and future of the Earth–Moon orbital system. *Planet. Sci. J.* **2**, 70 (2021).

151. Ray, R. D., Eanes, R. J. & Lemoine, F. G. Constraints on energy dissipation in the Earth's body tide from satellite tracking and altimetry. *Geophys. J. Int.* **144**, 471–480 (2001).

152. Kerswell, R. R. Upper bounds on the energy dissipation in turbulent precession. *J. Fluid Mech.* **321**, 335–370 (1996).

153. Kerswell, R. R. The instability of precessing flow. *Geophys. Astrophys. Fluid Dyn.* **72**, 107–144 (1993).

154. Lacaze, L., Le Gal, P. & Le Dizes, S. Elliptical instability in a rotating spheroid. *J. Fluid Mech.* **505**, 1–22 (2004).

155. Lin, Y., Marti, P. & Noir, J. Shear-driven parametric instability in a precessing sphere. *Phys. Fluids* **27**, 046601 (2015).

156. Kerswell, R. R. Tidal excitation of hydromagnetic waves and their damping in the Earth. *J. Fluid Mech.* **274**, 219–241 (1994).

157. Mineev, V. N. & Funtikov, A. I. Viscosity measurements on metal melts at high pressure and viscosity calculations for the earth's core. *Physics-Uspekhi* **47**, 671 (2004).

158. Touma, J. & Wisdom, J. Evolution of the Earth-Moon system. *Astron. J.* **108**, 1943–1961 (1994).

159. Neron de Surgy, O. & Laskar, J. On the long term evolution of the spin of the Earth. *Astron. Astrophys.* **318**, 975–989 (1997).

160. Grannan, A. M., Favier, B., Le Bars, M. & Aurnou, J. M. Tidally forced turbulence in planetary interiors. *Geophys. J. Int.* **208**, 1690–1703 (2017).

161. Barker, A. J. & Lithwick, Y. Non-linear evolution of the tidal elliptical instability in gaseous planets and stars. *Mon. Notices Royal Astron. Soc.* **435**, 3614–3626 (2013).

162. Monteux, J., Andrault, D. & Samuel, H. On the cooling of a deep terrestrial magma ocean. *Earth Planet. Sci. Lett.* **448**, 140–149 (2016).

163. Deguen, R., Olson, P. & Reynolds, E. F-layer formation in the outer core with asymmetric inner core growth. *Comptes Rendus Geosci.* **346**, 101–109 (2014).

164. Rubie, D. *et al.* Accretion and differentiation of the terrestrial planets with implications for the compositions of early-formed solar system bodies and accretion of water. *Icarus* **248**, 89–108 (2015).

165. Jacobson, S. A., Rubie, D. C., Hernlund, J., Morbidelli, A. & Nakajima, M. Formation, stratification, and mixing of the cores of Earth and Venus. *Earth Planet. Sci. Lett.* **474**, 375–386 (2017).

166. Landeau, M., Olson, P., Deguen, R. & Hirsh, B. Core merging and stratification following giant impact. *Nat. Geosci.* **9**, 786–789 (2016).

167. Bouffard, M., Landeau, M. & Goument, A. Convective erosion of a primordial stratification atop Earth's core. *Geophys. Res. Lett.* **47**, e2020GL087109 (2020).

168. Vidal, J., Cébron, D., Schaeffer, N. & Hollerbach, R. Magnetic fields driven by tidal mixing in radiative stars. *Mon. Notices Royal Astron. Soc.* **475**, 4579–4594 (2018).

169. Christensen, U. R. Geodynamo models with a stable layer and heterogeneous heat flow at the top of the core. *Geophys. J. Int.* **215**, 1338–1351 (2018).

170. Olson, P., Landeau, M. & Reynolds, E. Outer core stratification from the high latitude structure of the geomagnetic field. *Front. Earth Sci.* **6**, 140 (2018).

171. Gastine, T., Aubert, J. & Fournier, A. Dynamo-based limit to the extent of a stable layer atop Earth's core. *Geophys. J. Int.* **222**, 1433–1448 (2020).

172. Bono, R. K., Tarduno, J. A., Nimmo, F. & Cottrell, R. D. Young inner core inferred from Ediacaran ultra-low geomagnetic field intensity. *Nat. Geosci.* **12**, 143–147 (2019).

173. Biggin, A. J. *et al.* Strange fields: non-uniformitarian paleomagnetic records imply that the geodynamo process has been substantially perturbed on multiple occasions. In *AGU Fall Meeting Abstracts*, vol. 2020, DI006–0014 (2020).

174. Manglik, A., Wicht, J. & Christensen, U. R. A dynamo model with double diffusive convection for Mercury's core. *Earth Planet. Sci. Lett.* **289**, 619–628 (2010).

175. Takahashi, F., Shimizu, H. & Tsunakawa, H. Mercury's anomalous magnetic field caused by a symmetry-breaking self-regulating dynamo. *Nat. communications* **10**, 1–8 (2019).

176. Monville, R., Vidal, J., Cébron, D. & Schaeffer, N. Rotating double-diffusive convection in stably stratified planetary cores. *Geophys. J. Int.* **219**, S195–S218 (2019).

177. Mather, J. F. & Simitev, R. D. Regimes of thermo-compositional convection and related dynamos in rotating spherical shells. *Geophys. Astrophys. Fluid Dyn.* **115**, 61–84 (2021).

178. Tassin, T., Gastine, T. & Fournier, A. Geomagnetic semblance and dipolar-multipolar transition in top-heavy double-diffusive geodynamo models. *Geophys. J. Int.* **226**, 1897–1919 (2021).

179. Davies, C. J. & Greenwood, S. Thermo-chemical dynamics in Earth's core arising from interactions with the mantle. *EarthArXiv* DOI: 10.31223/X5MW4G (2021).

180. Pavón-Carrasco, F. J., Osete, M. L., Torta, J. M. & De Santis, A. A geomagnetic field model for the Holocene based on archaeomagnetic and lava flow data. *Earth Planet. Sci. Lett.* **388**, 98–109 (2014).

181. Panovska, S., Constable, C. G. & Korte, M. Extending global continuous geomagnetic field reconstructions on timescales beyond human civilization. *Geochem. Geophys. Geosystems* **19**, 4757–4772 (2018).

182. Usoskin, I. G., Gallet, Y., Lopes, F., Kovaltsov, G. A. & Hulot, G. Solar activity during the Holocene: the Hallstatt cycle and its consequence for grand minima and maxima. *Astron. Astrophys.* **587**, A150 (2016).

183. Nilsson, A., Holme, R., Korte, M., Suttie, N. & Hill, M. Reconstructing Holocene geomagnetic field variation: new methods, models and implications. *Geophys. J. Int.* **198**, 229–248 (2014).

184. Valet, J.-P., Meynadier, L. & Guyodo, Y. Geomagnetic field strength and reversal rate over the past 2 million years. *Nature* **435**, 802–805 (2005).

185. Ziegler, L., Constable, C., Johnson, C. & Tauxe, L. PADM2M: a penalized maximum likelihood model of the 0–2 Ma palaeomagnetic axial dipole moment. *Geophys. J. Int.* **184**, 1069–1089 (2011).

186. Cande, S. C. & Kent, D. V. Revised calibration of the geomagnetic polarity timescale for the late Cretaceous and Cenozoic. *J. Geophys. Res.* **100**, 6093–6095 (1995).

187. Aubert, J., Finlay, C. C. & Fournier, A. Bottom-up control of geomagnetic secular variation by the Earth's inner core. *Nature* **502**, 219–223 (2013).

188. Le Reun, T., Favier, B. & Le Bars, M. Experimental study of the nonlinear saturation of the elliptical instability: inertial wave turbulence versus geostrophic turbulence. *J. Fluid Mech.* **879**, 296–326 (2019).

189. Moffatt, H. K. *Magnetic field generation in electrically conducting fluids* (Cambridge University Press, 1978).

190. Roberts, P. H. & Soward, A. M. Dynamo theory. *Annu. Rev. Fluid Mech.* **24**, 459–512 (1992).

191. Chen, L. *et al.* The optimal kinematic dynamo driven by steady flows in a sphere. *J. Fluid Mech.* **839**, 1–32 (2018).

192. Cowling, T. The magnetic field of sunspots. *Mon. Notices Royal Astron. Soc.* **94**, 39–48 (1933).

193. Wicht, J. & Sanchez, S. Advances in geodynamo modelling. *Geophys. Astrophys. Fluid Dyn.* **113**, 2–50 (2019).

Author contributions

All authors contributed equally to the thinking and writing of the article. ML contributed particularly to the convection energy budget, NS and DC to precession energetics and dynamos, and AF to the review of geomagnetic data.

Acknowledgements (optional)

The authors thank James Badro, Yves Gallet, Stéphane Labrosse, Guillaume Morard, Andreas Nilsson, and Peter Olson, for useful discussions, and three referees for their most valuable inputs and suggestions.

ML was supported by the Programme National de Planétologie (PNP) of CNRS-INSU co-funded by CNES. NS, AF and HCN acknowledge support by the French Agence Nationale de la Recherche under grant ANR-19-CE31-0019 (revEarth). DC acknowledges support from the European Research Council (ERC) under the grant agreement no. 847433 (THEIA project).

Competing interests

The authors declare no competing interests.

Code Availability Statement

The authors declare the code for Figures 4 and 5 is available from https://doi.org/10.6084/m9.figshare.16722346.

Peer review information

Nature Reviews Earth & Environment thanks [Referee#1 name], [Referee#2 name] and the other, anonymous, reviewer(s) for their contribution to the peer review of this work.

Publisher's note

Supplementary Information

Supplementary information is available for this paper at https://doi.org/10.1038/s415XX-XXX-XXXX-X

Figure captions

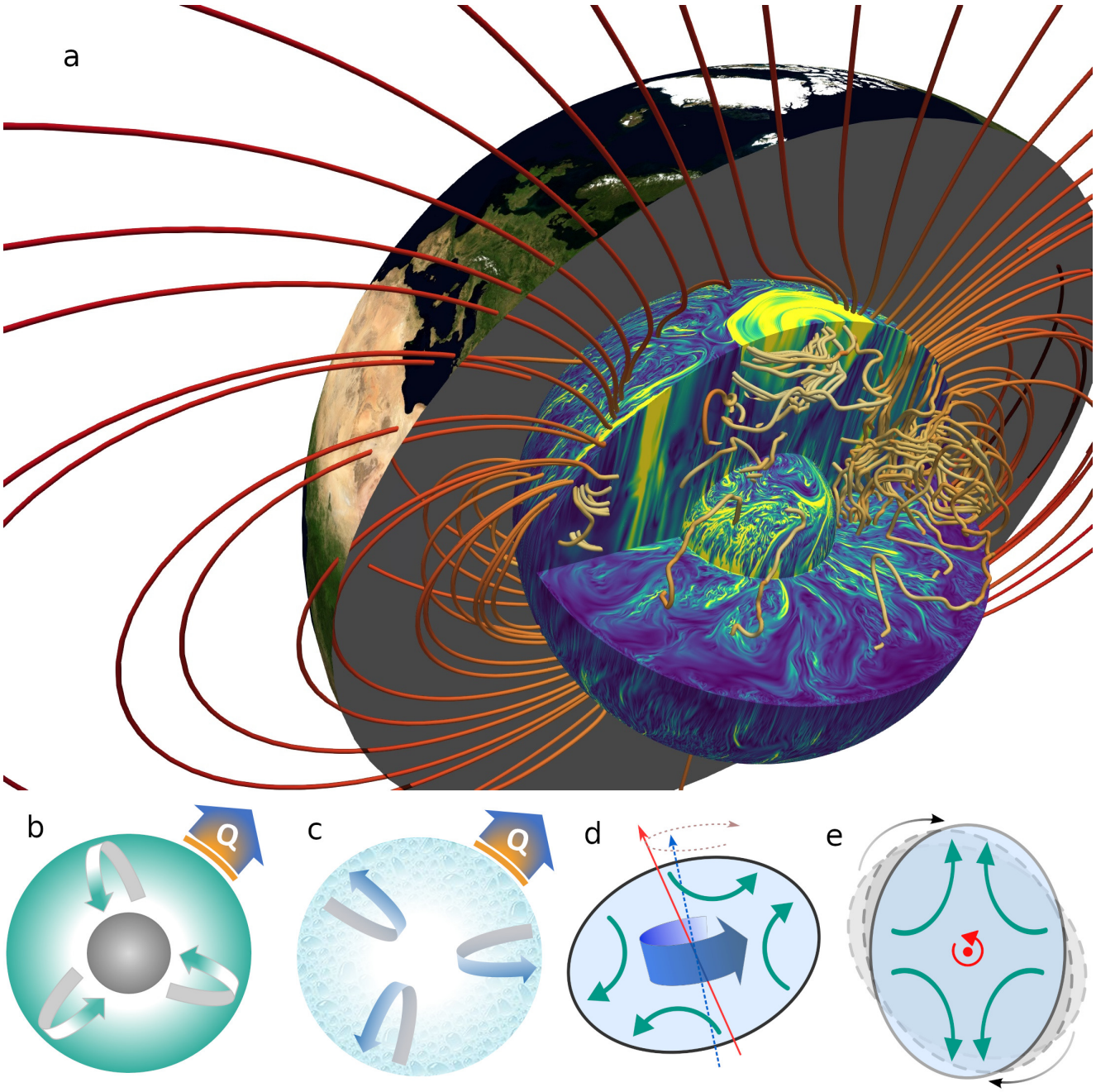

Figure 1. The Earth's dynamo requires turbulent motion of liquid iron in Earth's core. a| The three-layer structure of Earth's interior. The rocky mantle overlays a metallic core. The core, which is essentially made of iron, is divided into a liquid outer core and a solid inner core. The flow of liquid metal sustains dynamo action. The magnetic field lines (red to yellow lines) and the velocity field strength (blue to yellow) are taken from a direct numerical simulation of the dynamo driven by turbulent convection[11].

b-e| Candidate mechanisms to drive the geodynamo in the outer core. b| Convection driven by core cooling and inner-core growth. The heat Q_{cmb} leaving the core leads to the solidification of the inner-core, releasing light elements at the base of the outer core. At the outer edge of the core, cooling releases a cool, denser fluid that sinks into the deeper core. c| Convection driven by the exsolution of light oxides such as MgO or SiO_2. The iron-rich liquid released at the top of the core sinks into the core. d| Precession makes the fluid rotate along an axis (blue) that is different from the mantle rotation axis (red); a secondary circulation (teal arrows) is induced by the non-spherical shape. e| Tides induce a deformation that rotates around the liquid core in about 1 day, inducing a recirculation.

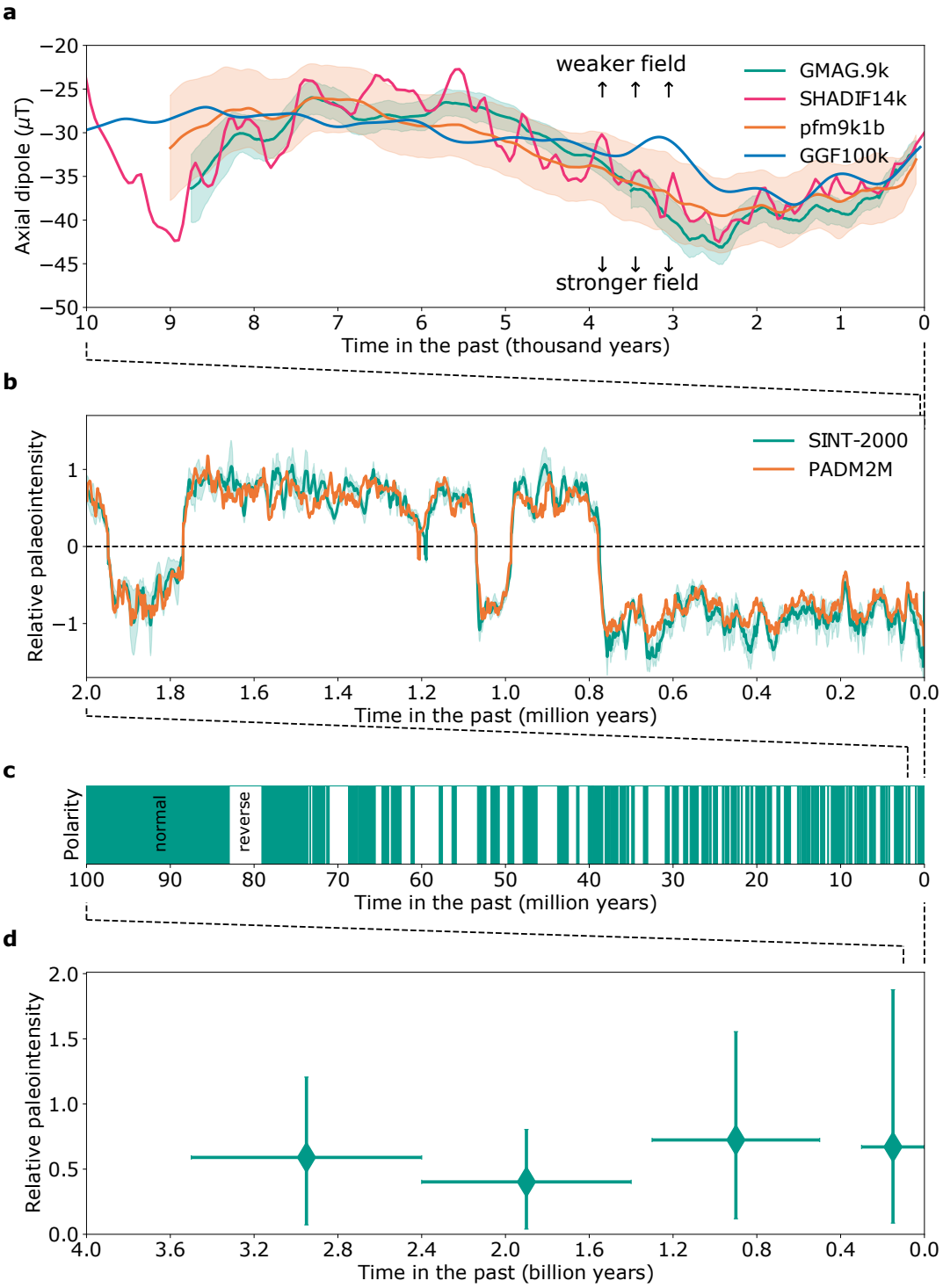

Figure 2. Earth's dynamo operates on a broad range of time scales. a| Evolution of the geomagnetic axial dipole (the g_1^0 Gauss coefficient) according to four reconstructions: SHADIF14k[180], GGF100k[181], GMAG.9k[182], and pfm9k1b[183], with the standard deviation uncertainty for the latter two. The axial dipole coefficient is given in μT. b| Fluctuation of the signed relative paleointensity of the magnetic field according to the SINT-2000 model[184], with its uncertainty, and the PADM2M model[185]. To normalise, the average virtual axial dipole moment $m_{\text{ref}} = 7.46 \times 10^{22}$ A m^2 since the last reversal is used. c| Geomagnetic polarity[186], showing the variability of reversal frequency. Intervals of normal (present-day) polarity are in teal. d| Virtual dipole moment from the PINT database[61], normalised by $m_{\text{ref}} = 7.46 \times 10^{22}$ A m^2. The coordinates of a symbol are the median value of the age interval and the median value of the dipole moment of the dataset selected for the time interval of interest. The horizontal bar spans the corresponding time interval, and the vertical bar covers the values found in the dataset. Historical geomagnetism and paleomagnetism provide key constraints on the operation of the geodynamo.

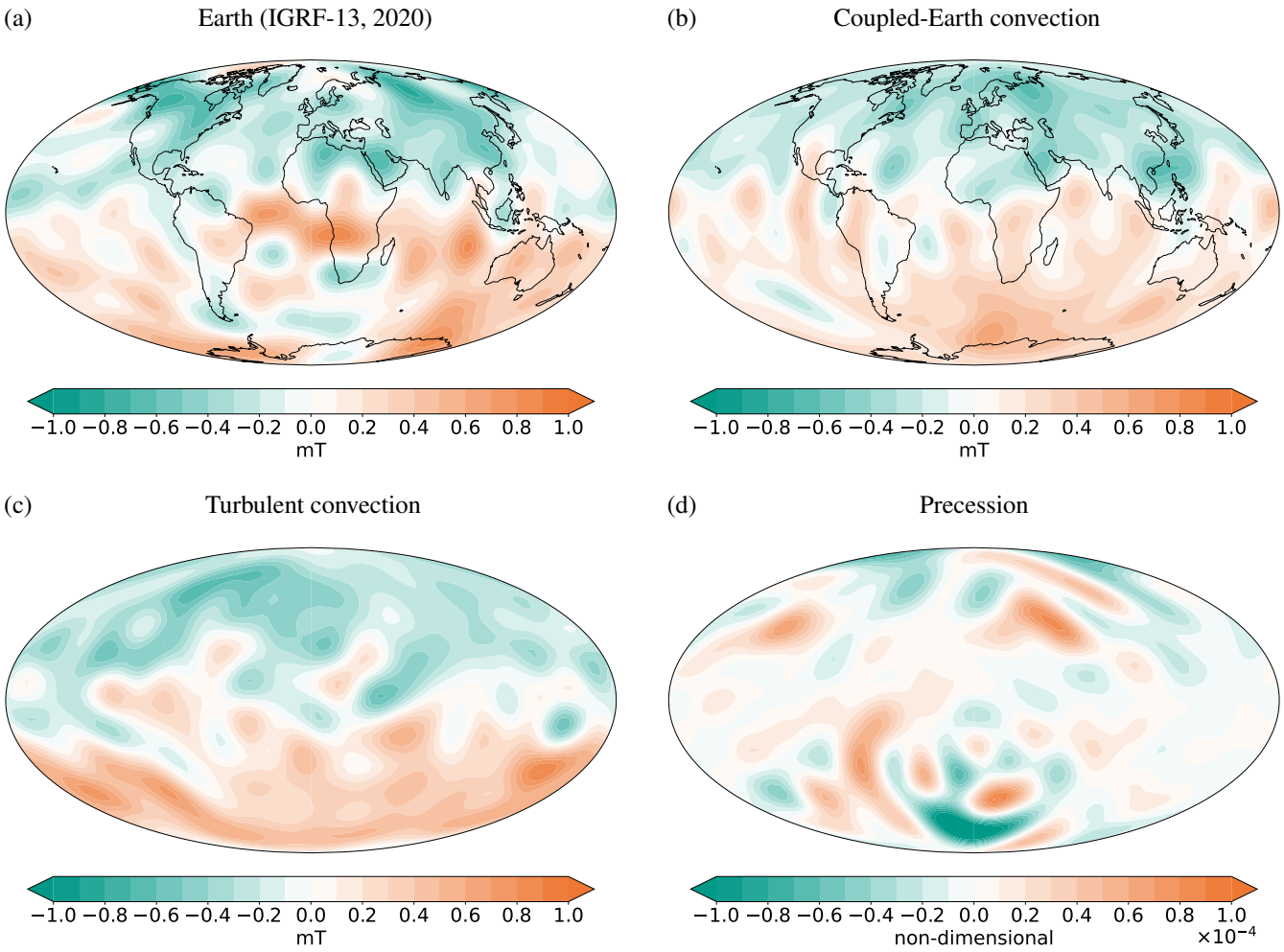

Figure 3. The morphology of the Earth's magnetic field is best reproduced by convection-driven dynamos. Snapshots of the radial component of the magnetic field at the core surface (Mollweide projection). Only the largest scales (spherical harmonic degree $\ell < 13$) that are resolved for the Earth's core are shown. a| Earth's magnetic field in 2020, according to the International Geomagnetic Reference Field model[46]. b| Coupled Earth direct dynamo model[12,187] ($Ek = 3 \times 10^{-5}$, $Rm = 930$, $Pm = 2.5$, see Box 2 for definitions), rescaled using dynamo scaling laws[187]. c| Direct numerical simulation[11], ($Ek = 10^{-7}$, $Rm = 514$, $Pm = 0.1$), rescaled so that the average axial dipole moment matches m_{ref}[184] (see Figure 2). d| Low-viscosity turbulent precession dynamo[105], aligned on the fluid rotation axis ($Ek = 10^{-5}$, $Rm \simeq 1900$, $Pm = 0.3$). Not all candidate driving mechanisms yield a magnetic field that complies with the observed field.

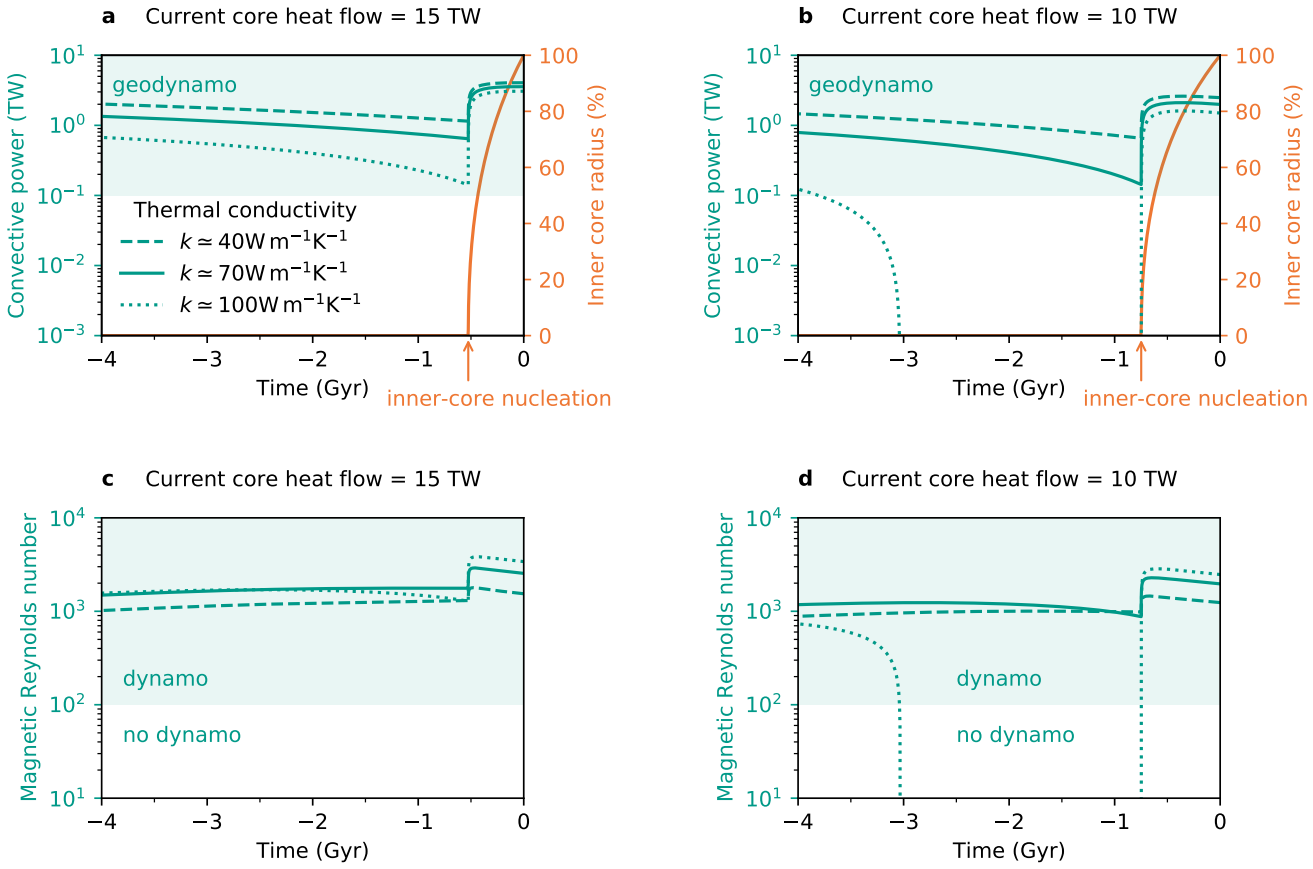

Figure 4. Convection can power the geodynamo in the distant past when thermal conductivity is lower than 100 $\mathbf{W\,m^{-1}K^{-1}}$. a| Convective power (teal) and inner-core radius (orange, % of its present-day value) generated by convection as a function of time. The shaded teal band delineates the range of admissible convective power for the geodynamo. A reduced model[121] was computed using three different thermal conductivities $k = 40$ (dashed), 70 (plain) and 100 $\mathrm{W\,m^{-1}K^{-1}}$ (dotted) corresponding to present-day conducted heat flows[27] $Q_{\mathrm{is}} = 6$ TW, 10 TW and 15 TW, respectively. The assumed present-day core heat flow is $Q_{\mathrm{cmb}} = 15$ TW. b| Same as a| with $Q_{\mathrm{cmb}} = 10$ TW. c| Magnetic Reynolds number Rm (see Box 1 and Box 2) generated by convection as a function of time for the same models as in a| ($Q_{\mathrm{cmb}} = 15$ TW). Dynamo action is expected only for $Rm \geq 100$ (shaded teal band). d| Same as c| with $Q_{\mathrm{cmb}} = 10$ TW. The core heat flow Q_{cmb} is arbitrarily assumed to increase at 2.9 $\mathrm{TW\,Gyr^{-1}}$, which is close to the lowest estimates from models that couple the thermal evolution of the core and mantle[127]. To compute the past evolution of the conducted heat flow $Q_{\mathrm{is}}(t)$ equations (1-2) and the evolution of core temperature from the energy budget of the core[120,121] are used. $Rm = U\,D/\eta$ is deduced from dynamo scaling law[12,135], where $U \simeq 2\,\Omega\,D\,p^{4/9}$ is the convective velocity, $p = \Phi_{\mathrm{conv}}/(\rho\,\Omega^3\,D^2\,\mathscr{V})$ the dimensionless convective power[84], Ω the time-varying Earth's rotation rate[158], $\mathscr{V}$ the outer core volume and D the evolving thickness of the outer core. The electric conductivity is assumed to depend on the thermal conductivity through the Wiedemann–Franz law. Convection provides enough power and kinetic energy to power the geodynamo over geological times.

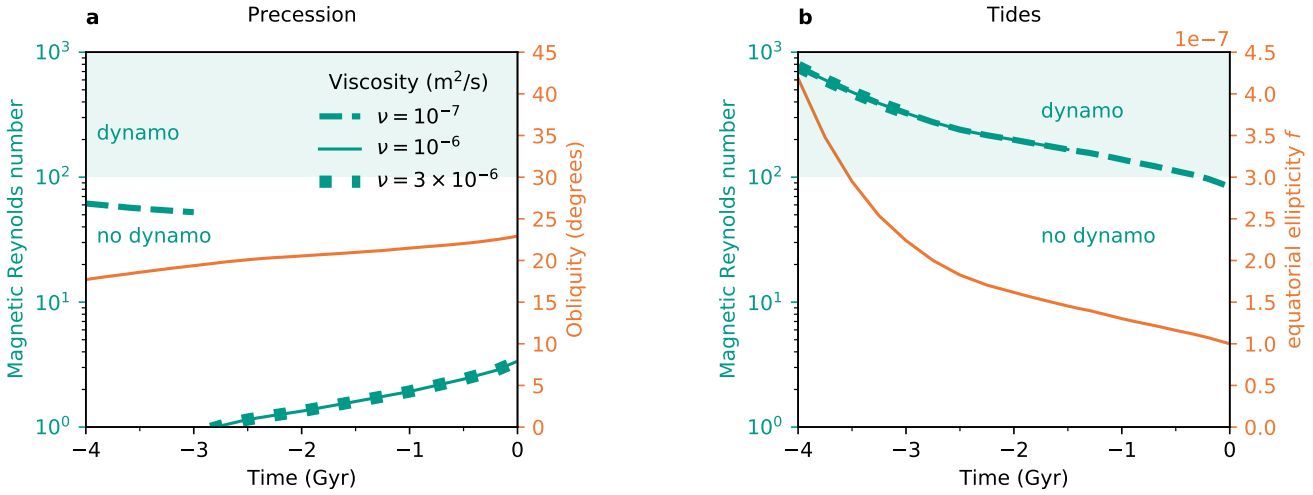

Figure 5. Precession cannot drive a dynamo but tides generated strong flows that could drive a dynamo in the early Earth. a| Magnetic Reynolds number Rm (teal lines, see Box 1) generated by precession as a function of time for three values[157] of the kinematic viscosity in the outer core. The Rm jump at -3 Ga for $\nu = 10^{-7}$ m^2/s is due to the triggering of bulk instabilities (instability onset is reached at this point). Dynamo action is expected only for $Rm \geq 100$ (shaded teal band). On the right vertical axis, the precession angle (obliquity) used for the calculation is shown. b| Same as a| for flows produced by tides but showing the equatorial ellipticity f used for the calculation on the right vertical axis. The estimates of Rm in b| are all associated with bulk instabilities, and the curves start at their respective onset for each viscosity. Criterion (10), with $K = 2.62$, is used to predict whether bulk instabilities are triggered. $Rm = U r_c/\eta$, where r_c is the core radius, is estimated using the following assumptions for the velocity, U. For times when bulk instabilities are excited, $U = f\,u$ is assumed, where u is respectively the differential velocity between the outer core and the mantle for precession and the speed of the tidal bulge at the core-mantle boundary for tides, and f is respectively the polar or tidal ellipticity[160,161,188]. For precession a|, for times -3 Gyrs to 0 when bulk instabilities are not excited, the flow velocity $U = 0.15\,\Omega\, r_c\, Ro^{3/2}$ is used for precession viscosity-driven instabilities[105], where Ro is the Rossby number $Ro = u/(\Omega\, r_c)$. Although precession could not have driven a dynamo in the Earth's history, tides could have driven a dynamo prior to 1.5 Gyrs ago.

Box 1: Basics of dynamo action

A dynamo converts mechanical energy into electromagnetic energy and produces a self-excited magnetic field[8,189,190]. The induction equation governs the evolution of the magnetic field $\boldsymbol{B}$ given the velocity field $\boldsymbol{u}$ of an electrically conducting but neutral fluid:

$$\partial_t \boldsymbol{B} = \nabla \times (\boldsymbol{u} \times \boldsymbol{B}) + \frac{1}{\mu\sigma}\nabla^2 \boldsymbol{B}, \tag{11}$$

with μ the magnetic permeability and σ the electrical conductivity. The above equation shows that the rate of change of the magnetic field results from the induction term (first term on the right-hand side), which involves the fluid motion and is responsible for the production of magnetic field, and the magnetic diffusion (second term on the right-hand side) related to ohmic dissipation. When induction is much larger than magnetic diffusion, a runaway growth of the magnetic field is possible. Comparing the order of magnitude of these two terms yields the dimensionless magnetic Reynolds number

$$Rm = \mu\sigma LU = \frac{UL}{\eta}, \tag{12}$$

with L the system length scale, U the typical fluid velocity, and $\eta = 1/\mu\sigma$ the magnetic diffusivity. A necessary condition to self-generate a magnetic field is $Rm \gg 1$. With U the maximum fluid velocity, the search for an optimal dynamo suggests $Rm \gtrsim 44$ in the sphere[191]. Another condition is that the velocity field is sufficiently complex and its topology adequate. For example, a solid-body rotation or strictly two-dimensional flows are incapable of dynamo action[192]. In contrast, helical flows are prone to dynamo action[9,191].

Such a dynamo process is different from the magnetic field produced by the motion of charged matter for which the field is simply proportional to the velocity and charge. In the case of a dynamo process, motions of a neutral fluid can lead to spontaneous generation of electric currents and magnetic field.

Box 2: Hard-to-reach dynamos

Multiple time scales control the Earth dynamo. The ordering of these time scales controls the regime in which the dynamo operates. When evaluated at the largest length scale, typical time scales range from a day for the rotational time to 10^5 years for magnetic diffusion.

The most relevant time scales are the rotation time $t_\Omega = 1$ day, the time $t_B = D\sqrt{\rho\mu}/B \sim 3$ yr of the hydromagnetic waves called Alfvén waves, the fluid overturn time $t_U \sim 300$ yr, the magnetic diffusion time $t_\eta = D^2/\eta \sim 10^5$ yrs and the viscous diffusion time $t_\nu = D^2/\nu \sim 10^{11}$ yr, where D is the outer core thickness, ρ the outer core density and ν the kinematic viscosity. Numerical simulations cannot cover such a range, but relevant regimes are reached when the ordering of these time-scales is preserved.

Dimensionless numbers evaluate the ratios between these times. These numbers are important to isolate the dominant physical processes. They are also necessary to properly compare numerical simulations, analogue experiments and Earth's dynamo (Supplementary Figure 1).

The magnetic Reynolds number introduced in Box 1 $Rm = t_\eta/t_U$ measures the importance of magnetic field production to magnetic diffusion.

The Ekman number $Ek = t_\Omega/t_\nu$ expresses the relative importance of viscous stress to the Coriolis force.

The Rossby number $Ro = t_\Omega/t_U$ quantifies the relative magnitude of inertial forces against the Coriolis force.

The magnetic Prandtl number $Pm = t_\eta/t_\nu$, is the ratio of kinematic viscosity ν to magnetic diffusivity η.

The Reynolds number $Re = t_\nu/t_U = Rm/Pm = Ro/Ek$ measures the degree of turbulence, that is the importance of inertial to viscous forces.

Estimates of these numbers for Earth's core are $Rm \sim 10^3$, $Ek \sim 10^{-15}$, $Ro \sim 10^{-6}$, $Pm \sim 10^{-6}$ and $Re \sim 10^9$. The values of Ro and Ek reflect the importance of planetary rotation on the dynamics. That of Pm is thought to be responsible for the scale separation between the large-scale magnetic field and the small-scale, turbulent velocity field.

The best way to assess whether a simulation is in the Earth's dynamo regime is to check that it does reproduce observed features of the Earth's magnetic field. The following table lists the current ability (marked with a ✓), or inability, (marked with a ✗), of convection-driven simulations, precession-driven simulations, and analogue experiments to account for selected properties of Earth's dynamo.

Feature	Convecting simulations[a] laminar/turbulent	Precessing simulations[a] laminar/turbulent	dynamo experiments (turbulent)
dipole-dominated field[b]	✓/✓	✓/✗	✓
surface morphology[c]	✓/✓	✗/✗	?
fast dynamics[d]	✗/✓	?	?
slow dynamics[d]	✓/✓	?	?
reversals[e]	✓/?	✗/✗	✓
strong-field[f]	✓/✓	✓/✗	✗
scale separation[g]	✗/✓	✗/✗	✓

[a] The simulations are separated into two classes, laminar and turbulent, which correspond to a ratio of inertial to viscous forces smaller or larger than $\sim 10^3$, respectively. [b] Dipole-dominated refers to a dynamo field whose main component is dipolar. [c] Surface morphology refers to the large-scale morphology of the geomagnetic field at the core surface, which is well-known down to a scale of 1500 km. [d] Fast dynamics refers to the presence of waves operating on the magnetic time scale t_B, which is substantially lower than the advective timescale t_U characterizing the slow dynamics of core flow. [e] Reversals refers to the capacity for the field to reverse its polarity in an irregular fashion over geological time scales. [f] Strong-field refers to a dynamo operating with a magnetic energy larger by several orders of magnitude than the kinetic energy. [g] Scale separation implies that the flow energy spectrum peaks at a scale much smaller than the dominant magnetic scale. For further details the reader can consult previous studies[15,105,193].